Stony Brook University

Non-Invasive Measurements of Bone Strain during Mechanical Loading using Pulsed Phase-Locked Loop Quantitative Ultrasound

A Thesis Presented

by

Frederick Serra-Hsu

to

The Graduate School

in Partial Fulfillment of the

Requirements

for the Degree of

Master of Science

in

Biomedical Engineering

Stony Brook University

December 2007

Stony Brook University

The Graduate School

Frederick Serra-Hsu

We, the thesis committee for the above candidate for the

Master of Science degree, hereby recommend

acceptance of this thesis.

Dr. Yi-Xian Qin (Advisor)
Professor, Department of Biomedical Engineering

Dr. Wei Lin (Committee Chair)
Research Assistant Professor, Department of Biomedical Engineering

Dr. Stefan Judex (Member)
Associate Professor, Department of Biomedical Engineering

Dr. Ted Lynch (External Member)
Technical Product Manager, Luna Innovations, Inc.

This thesis is accepted by the Graduate School

Lawrence Martin
Dean of the Graduate School

Abstract of the thesis

Non-Invasive Measurements of Bone Strain during Mechanical Loading using Pulsed Phase-Locked Loop Quantitative Ultrasound

by

Frederick Serra-Hsu

Master of Science

in

Biomedical Engineering

Stony Brook University

2007

Ultrasound has been widely used to non-destructively evaluate many kinds of materials, such as ceramics and metals with more recent applications in bone tissues. Quantitative Ultrasound (QUS) has been used to assess bone quality and fracture risk; providing a more informative technique than DEXA for osteoporosis diagnosis. A Pulsed-Phase Locked Loop device has been proven for accurate measurements of ultrasound velocity. This work sets out to determine if the time-of-flight ultrasound velocity tracking by the PPLL can give a measurement that is sensitive to bone changes during loading. The ability to non-invasively detect bone strains has many implications, including more accurate osteoporosis diagnostics and fracture risk determination using a true measure of bone quality. To test this methodology, phantom materials and cortical bone shells were both used in similar compression testing. The phantom materials varied in level of geometric complexity. In the simplest geometry, a rectangular block, the PPLL measurements showed very good sensitivity to the movement of the MTS piston head during material compression (R^2=0.928 ± 0.032). As the geometric complexity increased to solid and hollow cylinders, the sensitivity was still good; however the R^2 values dropped to 0.89 ± 0.21 and 0.54 ± 0.31, respectively. Cortical shells were cut from the mid-diaphysis of sheep femurs, prepared with 90° 3 element rosette strain gauges, and tested under compression. Two groups were created based on marrow cavity contents of either intact bone marrow, or water. The PPLL correlated well to local axial strain, with R^2 values of 0.70±0.27, and 0.62±0.29 for the marrow and water groups respectively. Despite good sensitivity, high variation, and non-normal distributions of data led to the creation of FE models to determine if ultrasonic path complications were arising. The FE models showed that the multiple paths cause received energy to be a superposition of signals, creating phase artifacts that can cause error in the PPLL measurements. Using these FE models, it was found that the PPLL correlates very well to local ultrasound path length changes. The systems sensitivity to loading in bone has been shown, and further work should take into consideration the conclusions from this experimental and numerical work.

Table of Contents

List of Figures and Tables

Acknowledgements

My gratitude extends first to Dr. Yi-Xian Qin, without whom this work could not have been completed. I thank him for his support and guidance in both academic and non-academic matters. His patience and encouragement are greatly appreciated.

I would like to extend my thanks also, to the scientists and staff and Luna Innovations. In my dealings and meetings with them they have been nothing but kind and helpful. I would especially like to thank Dr. Ted Lynch who provided insight and instruction for the current technology, and served as a member of my thesis committee.

Special thanks go to Dr. Wei Lin and Dr. Stefan Judex. Dr. Lin, was kind enough to help me to understand the principles of ultrasound, as well as serve as my committee chair. Dr. Judex offered statistical insight as well as served on the thesis committee. Along with other professors in the Department for Biomedical Engineering such as Dr. Clinton Rubin, they gave valuable feedback during meetings which allowed better understanding and analysis of the data obtained.

Without my fellow graduate students and post-doctoral students, I could not have completed this work. So I deeply thank all of them, especially Dr. Yi Xia, Dr. Jiqi Cheng, Dr. Anita Saldanha, Suzanne Ferreri, Hoyan Lam, Tao Peng and Adiba Ali. Numerous talks with Yi resulted in greater understanding, and analysis of the work at hand. Jiqi provided ultrasound and signals knowledge to me during the end of this work. Suzanne and Anita provided both guidance and ideas throughout the course of this work. Tao Peng aided in some of the experimental work. And both Hoyan and Adiba provided much needed support throughout the process. To you all, I extend best wishes and great success throughout your careers.

Lastly, I would like to thank my family. Their support allows me to continue down this educational journey. I owe it all to them.

Chapter 1: Introduction

1.1 Significance and Clinical Relevance

The adaptability of bone to its mechanical environment yields great diversity in bone strength. Both exercise and disease can have a profound effect on bone strength, and its ability to perform its necessary functions. The implication of a non-invasive bone strength diagnostic system reaches across the board from exercise, to rehabilitation, to disease diagnostics. For example, military regimes may be optimized using a system that tracks bone strength during training. As variable mechanical stimulation increases through running, jumping, jogging, etc, bone strength may be tracked upwards, until the regimen gets too intense and stress fractures begin to form, causing a loss in bone strength. In disease diagnostics, bone strength may be screened for, and used as a tool to provide early detection and determination of useful treatments. For osteoporosis alone, a system that is able to determine bone strength non-invasively could potentially be used to not only screen the 10 million Americans already suffering from the disease, but also the 35 million with osteopenia, and tens of millions of other people entering their 50s who are at risk for the disease.

This beginning work with the Pulsed Phase Locked Loop (PPLL) technique has many implications for future use and applications. The application of most interest in the current research is its use as an "ultrasonic strain gauge" that, if validated, allows the system to perform important measurements not only in diagnostic settings in bone diseases, but also in research settings where bone strain is desired.

Current techniques for measuring in vivo strain require invasive surgery to glue a physical wire strain gauge to the cleaned bone surface. The wound must then heal, with trans-cutaneous wires traveling from the gauge to the acquisition system. For grazers and lower quadrupeds like sheep, this technique can work, but still requires sterile surgery. For monkeys and chimps, the surgery can be done however the external wiring is often ripped off by the monkeys rendering the gauges useless. Only several attempts have been made to strain gauge human bones, including one done in Israel with only 2 soldiers. This technique, while useful, is very hard to justify in a research setting, and nearly impossible to justify in a diagnostic setting. With the development of the PPLL technique to monitor strain of hard tissue, the system may be adapted to track changes in bone during exercise, normal gait, jumping, load bearing, etc. This ability to track changes during exercise or lack-there-of can then be extended to possibly tracking degenerative changes in bone.

In the world of bone disease diagnostics, current methods rely on measurements like bone densometry (DEXA) and quantitative ultrasound (QUS). Densometry measurements provide only density, with little information about bone quality for instance. They are useful because over the decades that these measures have been taken, statistical studies have created thresholds where density measures can be used to infer information about osteoporotic fracture risk. Utilizing a QUS system can yield more accurate fracture risk predictions, due the physical nature of the ultrasound waves which pass through the material. The lack of ionizing radiation also allows QUS measurements to be taken earlier and more often. Once the PPLL technique is understood and validated, incorporating it into a QUS system could provide true mechanical information about the bone, and thus allow much more accurate diagnostics and fracture risk prediction.

The PPLL technique for analyzing bone could also penetrate multiple industries, allowing many different applications. This research is a first step towards validating and optimizing the technique for application as bone strain measurement system. It takes the first steps in determining how a system based on PPLL circuitry reacts during mechanical loading of bone tissue. Hopefully, at the end of this work it will be apparent that this technique is worth further investigation and has promise for great success.

1.2 Bone

The human skeleton is a living, dynamic tissue which responds to its environment and is essential for any functional mobility. The skeletal system is responsible not only for structural support, but also acts as a mineral reservoir for homeostasis; protects internal organs in the head, chest and pelvis; and takes part in hemopoiesis within bone marrow cavities. Understanding of bone biology and structure, composed of compact and trabecular (spongy) bone, can also help in the development of tools to diagnose both healthy and unhealthy states of bone tissue. [1, 2]

Compact bone represents about 80% of all bone in humans, and forms the outer layer of all bones, the shafts of long bones, and a cortex around vertebral bodies, thus it is also known as cortical bone. [2] Compact bone is organized into cylindrical units known as osteons, which orient themselves along the bone long axis At the center of each osteon is a Haversian canal which houses capillaries and nerves. Surrounding this canal are concentric layers called lamella, which have alternately oriented collagen fibers to help withstand torsional stresses. This orientation of osteons helps to withstand the compressive loads seen

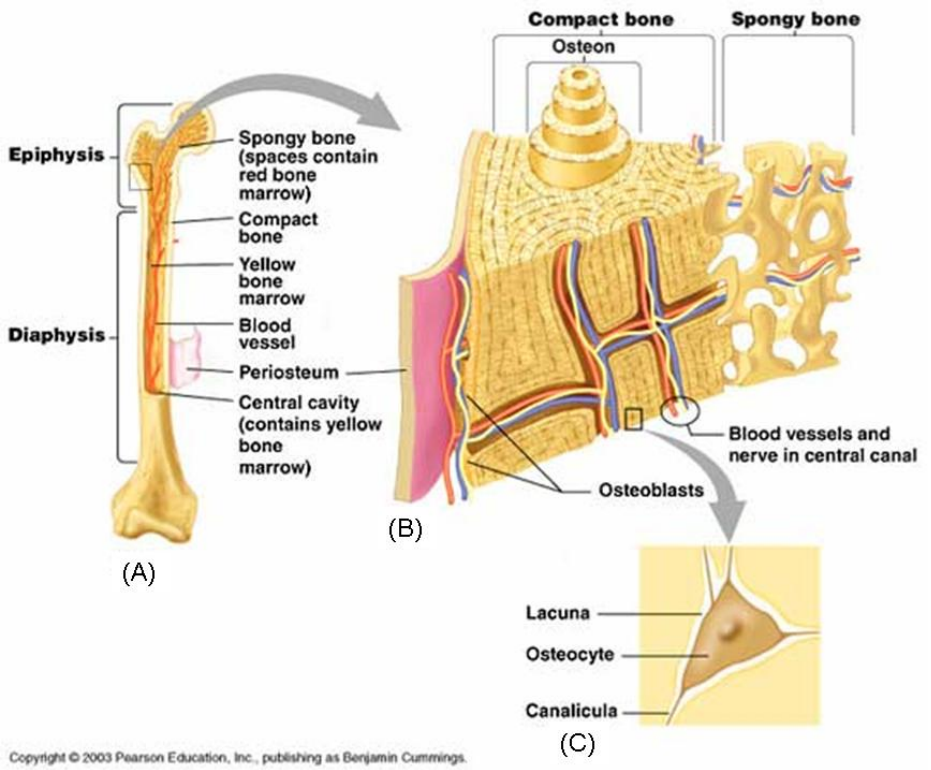

Figure 1.1: Bone Tissue Anatomy. The structure of the whole Femur (A) is a composite of tissue-level structures (B), with the small bone porosities seen in (C).

in bone. Several things make biological materials much more complex, and thus harder to nun-destructively test, than metals and inorganic composites. First, living tissues contain cells, which themselves can have a wide variety of properties. Bone contains a great variety of cells, not only in the bone tissue, but also in the marrow cavities of long bones, and in the porosities of trabecular bone. And like most organic materials, even compact bone has some amount of porosity. Organic material needs porosities for transporting all the necessary fluids and nutrients to sustain it as a living tissue. The porosities in cortical bone range from 1 mm in the Haversian canals down to 10μm in the lacunae, which connect the small pores that house osteocytes. The overall porosity of compact bone is only 5-10%, and its density of is around 1.9 g/cm^3. [2, 3] Acoustic determination of porosity and structure, and material properties of cortical bone has been completed in the past. It has been suggested that bone porosity can be linked to ultrasound velocity. As expected, an increase of ultrasound velocity was found as both porosity and pore size decreased. [4] Acoustic methods can be employed in determining mechanical properties of human cortical bone; which show anatomic site dependence. In the femur, modulus values range from 18.5-33.1 GPa, while acoustic velocities range from 3548-3967 m/s. [5]

Trabecular bone is characterized by a porosity of 75-95% with interconnected pores that fill with bone marrow, and has a much more variable density due to variations in porosity. The trabeculae themselves have been found to have a slightly lower density than compact bone, at 1.6-1.9g/cm^3. [3] These trabeculae consist of plates or struts approximately 200 micrometers thick which can be noticeably organized to disperse loads in the ends of healthy long bones, or can be more randomly organized in other locations. [2] The plates and struts of trabecular bone rarely form full osteons, since they are not large enough. Instead the main distribution of load comes through the complex network of individual trabeculae. Trabecular bone remodels faster than compact bone, mainly due to the much higher surface area exposed to marrow. [2] The microstructure of these types of bone has significant effects on their mechanical and acoustic properties. This trabecular network is very complex, and usually acts as a highly scattering and unpredictable media for acoustic signals.

1.3 Ultrasound

Ultrasound consists of acoustic waves which propagate at frequencies higher than humans are capable of hearing (above 20 kHz). It is a pressure wave which propagates through a medium based on particle interactions within the medium. As the wave propagates, particles within the medium are forced together creating areas of compression at positive peak wave pressure, and forced apart creating areas of rarefaction at negative peak pressure. The propagation speed of an ultrasonic wave is determined by properties of the medium through which the wave is traveling, specifically its density and stiffness. [6] This dependence allows for differentiation between materials based on the speed

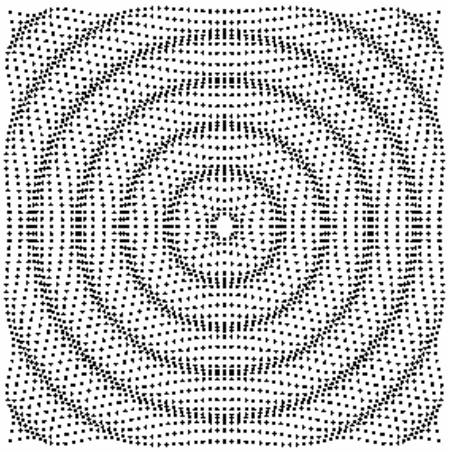

Figure 1.2: Sound waves radiating from a point source. Areas of compression and rarefaction can be seen clearly as particles are pressed together then accelerated apart as the wave energy moves through the material.

of sound through them.

In the case of elastic solids, both shear (S-waves) and longitudinal (P-waves) waves can exist. These two different waves travel with different velocities (c_s and c_p). With

$$c_p = \sqrt{\frac{(\lambda + 2\mu)}{\rho}},\ c_s = \sqrt{\frac{\mu}{\rho}}$$

being the velocities for longitudinal, and shear waves respectively, in terms of the solid's density, ρ, and Lamé constants λ and μ, which relate to Young's Modulus (E), Bulk Modulus (B) and Poisson's ratio (ν) by

$$E = \frac{\mu(3\lambda + 2\mu)}{\lambda + \mu},\ B = \lambda + \frac{2\mu}{3} \text{ and } \nu = \frac{\lambda}{2(\lambda + \mu)}.$$

In pathological processes which alter the material properties of biological tissue, if the ultrasonic velocity can be accurately measured, the result can be used to infer or diagnose that pathology. This is the basis for some current diagnostic devices for osteoporosis. [7, 8]

Acoustic waves interact with the medium through which it propagates, which gives rise to its usefulness in determining material properties. However this fact also lends itself to cause signal loss, and complications while attempting to take ultrasonic measurements and images. First, the wave energy can be absorbed by the material through which it propagates. Some of the energy used to moves the particles as the wave propagates is lost to heat energy, and can actually raise the temperature of the material. This heat increase is a constant concern, however can be effectively controlled by selection of the ultrasound energy intensity and wavelength. Second, like most waves, ultrasonic waves are subject to reflection and refraction governed by Snell's law. Reflection and refraction can cause problems when the ultrasound path must be determined, because unlike x-rays, this means ultrasound does not travel straight through a material. The refraction of a majority of signal energy out of the expected path can greatly increase the apparent attenuation of measurements. Attenuation is the loss of energy as the wave propagates through the medium. Reflection, scattering and absorbance are all modes of attenuation. Reflection and scattering actual refer to the same physical phenomenon of when energy is redirected away from the primary incident path. It is deemed scattering when wavelength is greater than or comparable to the object dimension. [6, 7] This is important in hard tissue, as wavelengths are often around 0.5-1.5 mm. Wave energy may be reflected at a cortical shell interface, however it will be scattered once it enters trabecular bone, due to the random angles at which it hits the individual trabeculae. This scattering inside trabecular bone causes large amounts of energy loss, however depending on the ultrasound frequency and intensity, it is still quite possible to receive a signal and amplify it to useable ranges without much noise introduction. Despite the problems attenuations causes with ultrasound signals, certain modes of energy re-direction have been utilized for positive results.

Acoustic scattering has found many uses in the medical field, the first of which was 2D brightness imaging. For ease of signal transmission and receiving, the main type of scatter used is acoustic backscatter, which reflects directly back into the direction it was coming from. In this mode, ultrasonic pulses are sent out, and the backscatter echoes are collected. Upon return, the magnitude of the reflected wave determines the brightness of the point on a screen, and as the waves are panned in 2D, an image will appear on the screen. The image relies completely on an assumed ultrasound velocity, so that the timing of a return pulse can be placed spatially on the screen. This can provide useful images of tumors, growths, and babies, but does not provide any material information. Much more recently,

this scattering has been investigated in its ability to determine porosity spacing by utilizing frequency domain approaches to analyze the repetitiveness of scattering events. [9-11]

The reflection of ultrasound can be used in nondestructive analysis of materials. [8] Just as in the 2D imaging modality described above, flaws of various sizes can be detected in materials by scanning the material with a wide range of frequencies. Just as important as flaw detection however, is material characterization. Nondestructive material testing has become a large industry where not only flaw detection, but actual mechanical properties can be determined. Recently this ability to determine elasticity and inelastic properties of materials has been turned towards biological tissues. The application of these nondestructive techniques to biological tissues became referred to as Quantitative Ultrasound in the medical fields.

Quantitative ultrasound (QUS) emerged with high promise in the early 1990s. QUS is based on obtaining quantitative information about the object and material in question, using the physical nature of ultrasound. Prior to this, the majority of medical ultrasound focused on imaging only, which cannot provide quantitative information. Some 15 years later, it is still clinically underutilized while in research increasing amounts of work continue to be done. Current commercial systems use speed-of-sound (SOS) and broadband attenuation (BUA) as their main measurement parameters. The exact nature of the bone properties measured is currently unclear in these systems, and only peripheral sites such as the calcaneus can be measured. That combined with the inability to use current DEXA thresholding for diagnosis has kept the use of these systems to a minimum. QUS measurements at the phalanges have shown SOS dependence on cortical area, density, and porosity. The SOS measurements had varying degrees of association with DEXA BMDs, but stronger relationships to these other skeletal properties. [12] Research is still being done in QUS, especially in the areas of QUS imaging, region selection, and backscatter analysis. Backscatter has recently been utilized to help predict trabecular number, and spacing with good results. [9-11] QUS still shows great promise, and a possible combination of precise PPLL measurements with QUS protocols may yield more accurate mechanical knowledge of bone for diagnostic purposes.

1.4 Pulsed Phase-Locked-Loop

Pulsed-Phase-Locked-Loops (PPLLs) are based primarily on the concepts of phased-locked loops. The phase-locked loop (PLL) was first developed in the 1930's, but only become widely used after its emergence as an integrated circuit (IC) in the 1960's. This PLL IC is responsible for many things taken for granted today, such as the constant color of pixels in televisions, and de-modulating frequency-modulated signals like the ones found in FM radio. The ability of these circuits to very accurately determine and react to the phase difference between two signals makes them a very useful control mechanism, for example, in constant speed motors. The phase-locked loop has three basic modules: the phase detector, the loop filter and the voltage controlled oscillator. [13]

The phase detector can be a variety of components, the simplest of which is an analog multiplier. The simple multiplier is not only one of the simplest of phase detectors, but is also quite widely used in PLL implementation, and therefore will be used to describe PLL function. The multiplier takes two signals and multiplies their values at each instant in time, generating a signal with twice the input frequency and a DC offset proportional to the phase difference between the two signals. More precisely, the DC offset is proportional to how far the phase shift between the two signals differs from pi/2, as the simple multiple of two

sinusoids oscillates about zero when they are 90 degrees out of phase. From now on, for the purpose of PLL introduction "in phase" will be considered to mean 90 degrees out of phase, such that multiplier output is zero.

The output signal from the multiplier is then passed through a low-pass filter to remove the unwanted oscillations, allowing only the DC component through to the voltage controlled oscillator (VCO). The VCO is controlled by a constant voltage source plus whatever voltage is output from the filter. Thus, if the input signal jumps ahead in phase, the VCO will increase its oscillation frequency to drive the leading edge of the waveform towards the multiplier faster. As the signals become closer and closer in phase, the multiplier out becomes smaller and smaller and the VCO moves closer and closer to its original constant frequency. This circuit thus "locks" two signals in phase, not allowing either to digress to far, for to long. Although the basic PLL description seems simple, design and implementation requires knowledge beyond the scope of this project. In addition, implementation of the PLL in a pulsed ultrasonic measurement system requires much more complex electronics.

The Pulsed-Phase-Locked Loop circuitry contains much more than the three basic components described above. However the system used is proprietary information, and therefore will be excluded from this introduction. Instead a general PPLL from older patents will be described in brief detail for the sake of understanding how the measurements in the next few chapters were obtained. The signal originates in the VCO and is subsequently split

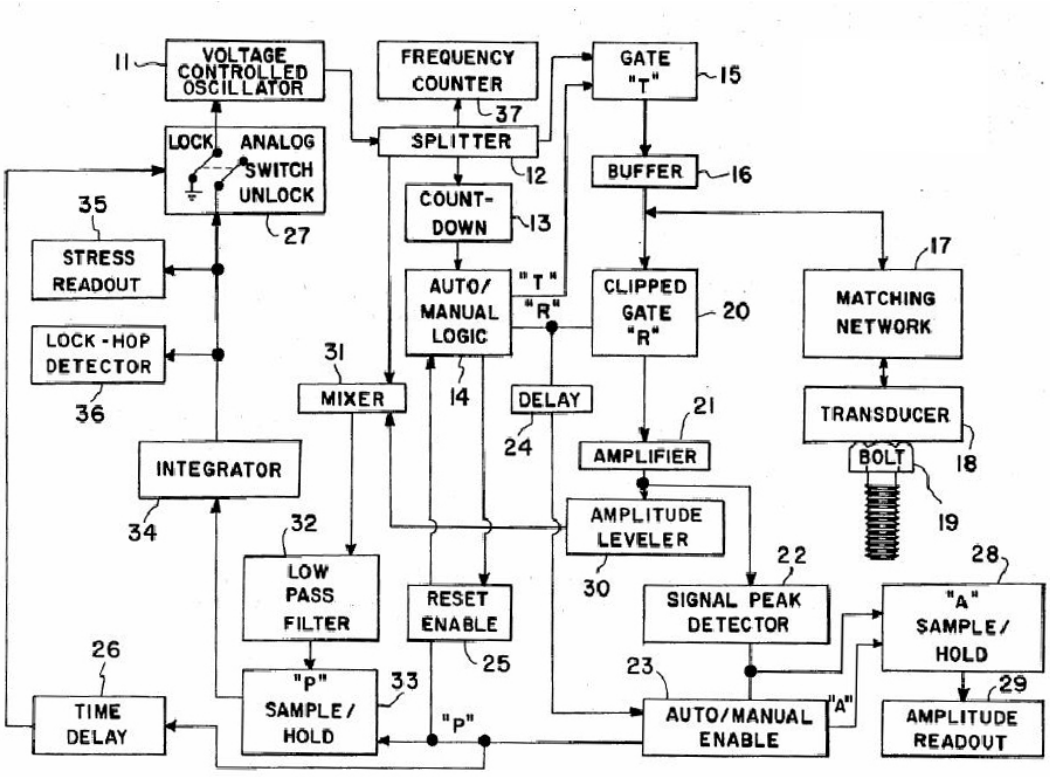

Figure 1.3: Patented PPLL Circuit design, from US Patent Number 4363242, for a Pulsed Phase Lock Loop Strain Monitor. This is not the device used in current research, but is now public domain and is useful in understanding the necessary components. The current device is currently the property of Luna Innovations, Inc. (Hampton, VA).

into 4 isolated signals. One of these signals enters into a counter circuit which releases a pulse after a certain number of cycles. This pulse is used to control a logic circuit which opens and closes a transmitter gate. A second identical signal from the VCO is sent through the transmitter gate when it is closed by the logic circuit. This signal is then amplified and used to drive an ultrasonic transducer. The signal is then received and collected through a gate which is controlled by the same logic circuit as the transmitter gate (in pulse-echo mode). After amplification, this signal is sent directly to the phase detector. The output from the phase detector gets filtered and then sent to a sample and hold circuit, which takes the output of the phase detector and samples it when the pulse is being received from the transducer, and holds that level when there is no pulse to compare phase with. After the sample and hold circuit, the output can go directly back to the VCO, however some systems offer control on the phase set point. This allows the user to set the desired phase shift in a circuit which introduces its own DC offset proportional to the phase offset the user decides. This DC offset is added to the output from the phase detector and is then sent to the VCO. The option to "unlock" or "lock the system can come from a simple user operated switch placed between the sample and hold circuit and the VCO. As stated above, the VCO output is split into 4 isolated signals. The fourth is sent to a frequency counter which outputs the signal frequency. The VCO frequency is the value measured during testing with this PPLL technique. [14]

1.5 PPLL and Physical Measurements

The pulsed phase lock loop uses changes in signal phase in a feedback loop to control the oscillator frequency. As the frequency changes, we know the phase has changed between the reference signal and the ultrasonic signal put through the sample. But what does this mean physically? As the phase dependent frequency changes, the time-of-flight (TOF) velocity of the ultrasound wave is changing. If the velocity drops slightly, the expectation is that the reference signal will be slightly ahead in phase, which would in turn cause the frequency to drop until the two signals are in phase again. This may be counter intuitive, because ultrasonic testing transducers are designed to give maximum power at a certain frequency. So altering the excitation frequency might then alter the power output of the transducer which may cause measurement problems, and thus give rise to false phase shifts. However in these systems, the frequency is changed only very slightly during phase shifts, on the order of tens to hundreds of Hz in this experimental setup. With a central frequency of 2.25 MHz, changes in hundreds of Hz, while measurable with a simple frequency counter, are assumed not to exceed the transducers capabilities.

It may not be intuitive to alter the frequency at all, when comparing a signal of reference speed, to a signal of variable speed. Why alter the frequency of the reference, when the speed is what has caused phase changes? There is no simple way to change the speed of an electrical signal; however it is very simple to alter the control voltage to the VCO based on the output from the phase detector. This variable frequency thus corresponds to some change in TOF velocity in the ultrasonic path (See section 1.3). Physically, this gives us a useful tool for measuring and tracking TOF velocity and with some assumptions can yield information about the acoustic state of things along the ultrasonic path.

In the current application there are two main methods that can change the TOF velocity of the propagating ultrasound. First, and hopefully the more influential, is the geometric change in path length of the ultrasound. As the transducers are fixed, this is not an

absolute change in length, but a relative change in length traveled through water versus length traveled through the sample material. Under compressive loading the sample will alter its dimensions, which will cause the ultrasound TOF to change. The alternative method of TOF velocity change is a physical change in the material properties of the material. A change in density or modulus will result in a different natural sound speed in the material causing a shift in TOF velocity. The following work will focus on the first method of TOF modulation.

Theoretical relations between changes in PPLL frequency and changes in ultrasound path length have been previously developed and tested. Cantrell et al. provides a good derivation of this simple relation,

$$\frac{\Delta f}{f} = \frac{\Delta c_p}{c_p} - \frac{\Delta l}{l}$$

from basic phase relationships, where f is the measured VCO frequency, c_p is the phase velocity, and l is the ultrasonic path length. This relation has been tested for temperature dependent ultrasonic wave velocity measurements in water. [15] The actual derivation is less important to this work than the assumptions made to get there. The two main assumptions used by Cantrell and utilized here are that; A, the system phase does not vary as a function of frequency and B, there is no change in state of quadrature during measurement. If the system phase varied with frequency, then there would need to be corrections for system phase artifacts while taking frequency measurements. And, if there is a change in the quadrature state during experimental measurements, then there would be a large jump in frequency not related to actual phase shifts. These assumptions have been used for similar variable frequency PPLLs in the past, therefore this relation may be validated for this system once the current setup has been shown to provide consistent responses. If validated, using this relation it can be seen that using phase velocity and frequency measurements, may allow the back calculation of a change in ultrasonic path length.

1.6 Current PPLL Applications

The phase-locked-loop has implanted itself solidly in dozens of applications since its emergence as an integrated circuit in the 1960s. However the pulsed phase-lock-loop is really limited to applications where signal bursts are necessary. This ability to send out bursts lends itself well to applications in ultrasound, given its ability to keep the duty cycle on transducers low and signal interference to a minimum. Acoustic PPLLs have found uses in applications from studying the anelasticity of metals to tracking changes in intracranial pressure (ICP). Recent medical applications such as ICP tracking or intramuscular pressure sensing have only emerged very recently. The first patents filed for PPLL measurement systems go back to the early 1980s. [14, 16-20] These early bolt tension measurement systems are the basis for more modern PPLL measurement systems.

Current applications of the PPLL technology in the medical field include intracranial pressure measurements, and most recently investigations into compartment syndrome. [21-27] In 2005 Uneo et al. published a technical note on the “Noninvasive assessment of intracranial pressure waveforms by using pulsed phase lock loop technology.” Based on the fact that the skull diameter actually varies proportionally to the intracranial pressure, it was hypothesized that the PPLL could measure variations in the skull diameter which can then be used to calculate ICP. While the distance of variation is small (on the order of several microns) it can translate to large changes in the phase difference of the reflected signal. A

500 kHz transducer was used to transmit signals from one side of the skull, and then receive the reflected signal from the inner surface of the opposite side of the skull. The overall correlation between PPLL measures and invasive ICP measurements was reported as 0.88 with a standard error of 0.02. For this application, the ICP signal dynamics are important clinically, and to determine how well the PPLL waveform dynamically follows the ICP waveform, coherences were calculated at different harmonics of the standard heart rate. These coherences yielded R^2 values of greater than 0.6, and therefore ICP waveform dynamics were closely followed by the PPLL measurements. While the PPLL measurements cannot be directly converted into actual pressure, in the clinically setting the ICP waveform dynamics are important, and so it is a unitless waveform with very similar dynamics. The results from this work show strong support for the use of the PPLL technique as an ICP measurement device in the clinical setting. This technique is one of the first successful applications of the PPLL technique to the medical world. [22] More recently, applications to investigate intra-muscular pressure (IMP) and compartment syndrome have surfaced. In a recent clinically study, Wiemann *et al*. showed that the increases in IMP correlates linearly to PPLL measurements of muscle membrane displacements during arterial pressure pulsations, with an R^2 of 0.889. [21]

1.7 Objective and Specific Aims

The PPLL has proven itself effective in measuring the temperature dependence of ultrasonic velocities in water. [15, 20, 28, 29] It has also been shown to measure cranial dilation sensitively enough to closely correlate to dynamic intracranial pressure. [16, 22, 23, 25, 27, 30] Recent developments in scanning QUS systems can provide very good diagnostics for osteoporosis. [12, 31-36] These systems, coupled with the sensitivity of the PPLL could possibly yield true mechanical information about hard tissue, and might thus provide the best possible non-invasive diagnostics for bone disease, and rehabilitation. **The overall objective of this work is to determine if an ultrasonic system, utilizing the PPLL technique could be sensitive enough to detect changes in bone during loading in their elastic range, thus providing a means of calculating bone mechanical properties.** The above objective will be completed in phantom material and cortical bone samples, utilizing an MTS Minibionix 858 axial loading device (MTS Corporation, Eden Prairie, MN) and a prototype PPLL device courtesy of Luna Innovations, Inc. (Hampton, VA). The main objective will be achieved by the following three specific aims.

Specific Aim 1: To evaluate the sensitivity of the PPLL to changes seen in simple phantoms during compressive loading, and determine how well the PPLL can correlate to variables acquired by the loading apparatus, specifically MTS piston head displacement.

Specific Aim 2: To evaluate how well the PPLL measurements correlate to loading variables, and local strain measurements in cortical bone samples. The variables of interest are the local axial, and circumferential strain and an estimation of the ultrasound path-length change, based on surface strain measurements.

Specific Aim 3: To determine whether the PPLL more closely tracks dimensional changes along the ultrasound path direction, utilizing Finite Element Modeling to extract internal path-length changes seen during loading of the cortical specimens in specific aim 2. The PPLL should be most sensitive to changes in dimension along the internal ultrasound paths, thus, FE models of individual bone geometries will be used to extract these internal changes during each stage of loading.

Chapter 2: PPLL Technique Sensitivity in Phantom Materials and Simple Geometries

2.1 Introduction and Rationale

Non-destructive testing of materials using ultrasonic investigation is a well established field; however only a few applications into living tissues have been explored. Recent advances in Quantitative Ultrasound (QUS) have allowed for more accurate evaluation of bone quality and fracture risk associated with bone diseases such as osteoporosis. [11, 12, 32-36] Current QUS techniques, however, are still based on correlative methods and use ultrasound based parameters such as attenuation, velocity and broadband attenuation, to make predictions about material properties. Traditional mechanical properties (i.e. modulus) still require either destructive testing or at the very least, invasive attachment of strain monitoring devices during loading protocols. Pulsed Phase-Locked-Loop (PPLL) systems are based on the phase-locked-loop circuitry which was first investigated during the 1930's. [13] The incorporation of the PPLL circuitry into ultrasound systems has allowed for very precise measurement and monitoring of ultrasound velocity through a medium. With such precise monitoring of ultrasound velocity changes it may be possible to detect the time-of-flight velocity variations during the loading of material. With this ability it would be possible to associate applied loads with measured levels of strain in the material, without invasive measurements.

The overall objective of this research was to apply PPLL technology to the monitoring of bone tissue during loading, by first establishing that the technology responds to phantom materials. As in most imaging and diagnostics, phantoms are used to gradually step up the complexity of the problem at hand, to determine performance criterion and illuminate specific sources of error. In this case phantom materials can be made to simple geometries, and can be repeatedly tested to evaluate system consistency. The first specific aim of this research is thus to test the responsiveness of the PPLL technique during mechanical loading of phantom materials. This work will show if the PPLL technique can provide a measurement that is highly correlated with loading variables measured by the MTS.

2.2 Experimental Setup

To efficiently answer the question of whether or not a PPLL based technique was capable of measuring a material response to loading; three different phantoms were used. The phantoms included one solid rectangular, flat surface phantom, and two cylindrical phantoms. The flat surfaced phantom was used to provide the most basic geometry, and base for all more complex measurements. The flat surface provides very little chance for ultrasound refraction, theoretically allowing the simplest ultrasonic wave propagation. This should allow the responsiveness of the PPLL to be determined before the effects of geometric complexities are introduced. The geometry of the cylindrical phantoms was used to match to geometry seen in the cortical shafts of long bones. To better mimic bone geometry, one phantom was hollowed out, creating a uniform plastic shell.

Phantom Preparation:

The solid rectangular phantom was cut from a high molecular weight polyethylene bar (McMaster-Carr, Part#9329K54). The final dimensions of the sample were 6x3x2.54 cm. This phantom was precisely cut and tested with direct contact to the MTS piston, thus no further preparation was needed. Two cylindrical phantoms were cut from hard plastic rod

stock with a diameter of 1.9 cm (3/4 in) to a length of 6 centimeters. One of these phantoms was kept as a simple solid cylinder for testing. The second phantom was hollowed out using a drill press in order to mimic the geometry of the cortical shell found in sheep femurs (wall thickness 4.8 mm). To ensure even load distribution from the mechanical testing apparatus, each contact end was embedded in self-curing acrylic. For the hollow cylinder a small hole was drilled in the acrylic so that during testing the inner cavity could be filled with vacuumed water for acoustic coupling.

Mechanical Loading Protocol:

The response of the PPLL system was investigated with a static loading protocol. This protocol was delivered to the phantoms with a MTS MiniBionix (MTS Corporation, Minneapolis, MN) axial load frame controlled with their TestStar II software. Due to its higher mechanical properties, the flat surface phantom was subjected to higher loads and its static loading protocol began with a 50N preload. Eight loads were applied for 5 seconds and then returned to the 50N reference for an additional 5 seconds. The loads applied were as follows: 100, 200, 300, 400, 500, 600, 700 and 800N, as seen in figure 2.1. The cylindrical phantoms were subjected to a similar protocol, starting with a 50N preload. However, the cylindrical phantoms were only subjected to five loading phases, each containing 10 seconds of a 50N reference load followed by 10 seconds of the peak load. The five peak loads applied to the cylindrical phantoms were 200, 300, 400, 500 and 600 N. All loads regardless of phantom used were applied as step loads under load control.

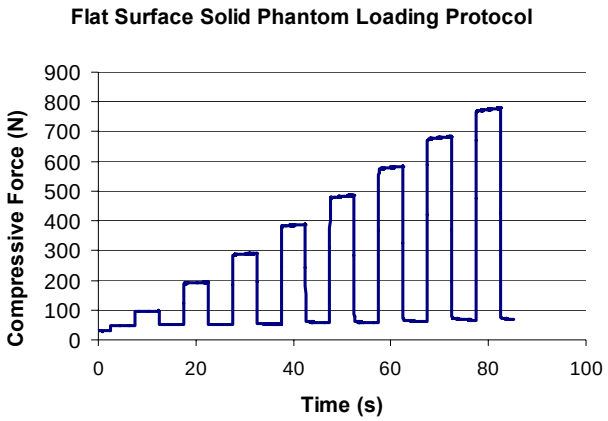

Figure 2.1: Flat Surface Phantom Loading Protocol. The loads are slightly less than desired with the MTS under load control.

Test Setup:

The PPLL system used was one of several prototypes built by Luna Innovations, Inc (Hampton, VA). The system consisted of two 0.5 inch diameter immersion transducers with a central frequency of 2.25MHz that were used to generate and receive the ultrasound signal. The transmitting transducer was focused and had a focal length of 0.5 inches. The receiving transducer was a plane transducer. The phantoms were each tested under the same setup which can be seen in figure 2.2. The sample and transducers were placed in a small bath containing de-gassed water for acoustic coupling. The transmitting transducer was connected directly to the PPLL supplied by Luna. The receiving transducer was connected to an amplifier which in turn sent the received waveform to both an oscilloscope and back to the PPLL device. The oscilloscope was mainly used to ensure that the received signal was present and did not get amplified beyond the magnitude accepted by the PPLL. The variable frequency PPLL device sent a reference signal to a frequency counter for data acquisition. The data acquired for each test included the frequency from the PPLL, and the load and piston displacement from the MTS. National Instruments Labview with a Dell 700m laptop was used to drive the PPLL and acquire the PPLL frequency. MTS Teststar IIs software

installed on a Dell Optiplex GX110 was used to control the MTS and acquire MTS variables. To ensure data acquisition began at the same time on both systems, an external trigger was used to begin the mechanical loading protocol and data acquisition. The sample was loaded with the MTS in the axial direction of the cylinder, while the ultrasound transducers were held in the water bath transverse to the axial direction. Therefore, any change in ultrasound path length investigated by the PPLL would be in the transverse direction to loading, and a result of material expansion during compression.

The flat surface phantom was tested 5 times consecutively, where the PPLL was stopped and restarted in-between each test. The only variable that changed as a result was the PPLL lock-point, since the sample was not moved within the acoustic field. The cylindrical phantoms were each tested a total of 20 times. These were divided into 4 test groups for each cylindrical phantom. Two of the 4 groups were tested with the sample in the same orientation with respect to the transducers. The other 2 groups were rotated by 90°. These two transverse orientations are theoretically identical (since the phantoms are cylinders), however the movement of the sample in the acoustic field may show variations, and thus the data for all batches of 5 consecutive tests are kept separate. Any variations in the system may show dependence upon sample placement within the ultrasound path. This yielded 8 groups of cylindrical phantom data as seen in Table 2.1.

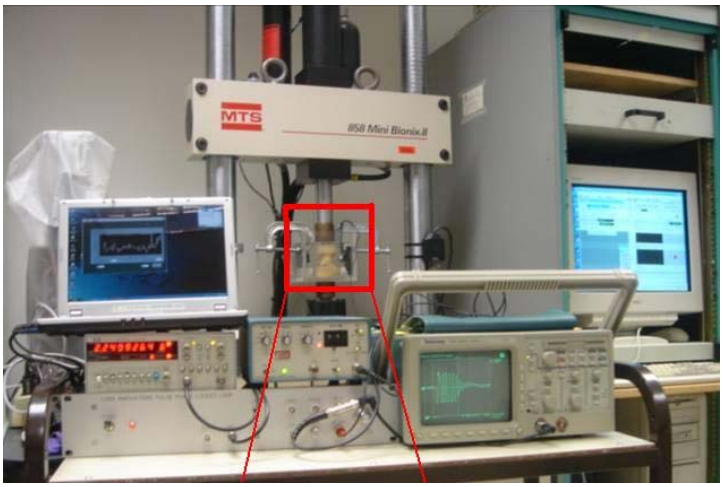

[2.2.A]

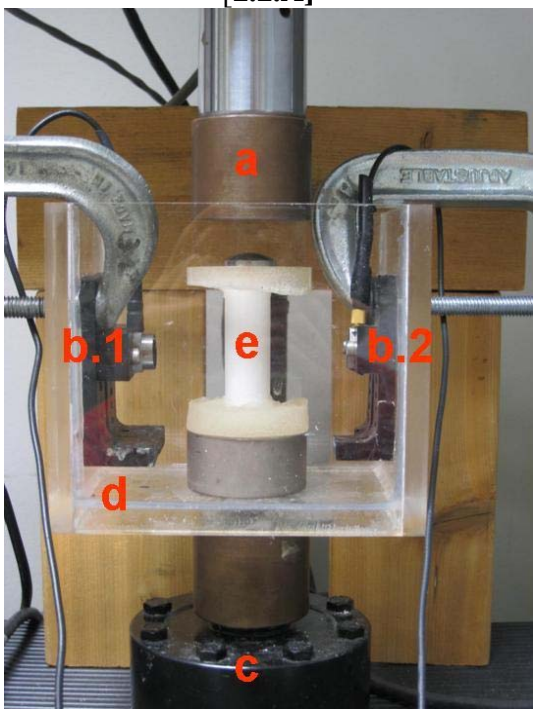

[2.2.B]

Figure 2.2: The total layout [A], showing the PPLL controller and acquisition laptop on top of the frequency counter, the Panametrics amplifier, and on bottom, the Luna Innovations PPLL. The MTS load frame holds the sample and PPLL transducers, the oscilloscope displays the received ultrasound signal, and the computer on the right controls the MTS and MTS variable acquisition. The cutout [B] shows the transducers (b.1,b.2) in their custom holders, held in place by the c-clamps. The sample (e) sits in the water bath, on top of the load cell (c), and loaded axially by the MTS piston (a).

Group Name	Phantom Tested	Orientation of Group	Batch Number
S.1.1	Solid	1	1
S.2.1	Solid	2	1
S.1.2	Solid	1	2
S.2.2	Solid	2	2
H.1.1	Hollow	1	1
H.2.1	Hollow	2	1
H.1.2	Hollow	1	2
H.2.2	Hollow	2	2

Table 2.1: Group information for individual batches of tests. Each batch contains data from the 5 consecutive tests run, without any movement of specimen.

Data Analysis:

All data were analyzed with custom written MATLAB scripts. Frequency data acquired from the frequency counter was sampled at approximately 30Hz; however it must be noted that time between samples was not perfectly constant (Fig 2.3). For this reason, MTS data were acquired at 100Hz, and down-sampled using custom MATLAB re-sampling algorithms to find MTS variable values at each of the time points at which a PPLL frequency value was obtained.

This re-sampling algorithm worked by linearly interpolating between the two MTS data points which occurred just before and after the point in time at which the frequency counter took a sample. Both linear and cubic fits to data were tried, however, due to the high sampling rate of the MTS compared to the PPLL frequency counter; there was no apparent benefit to using cubic interpolation.

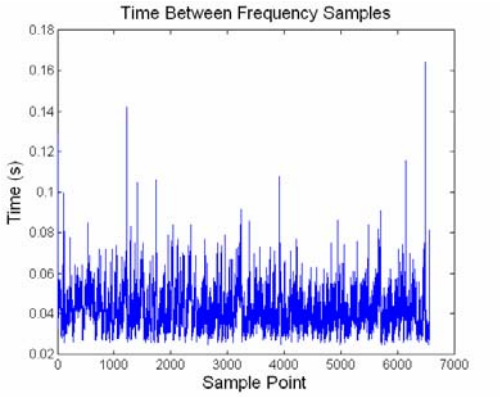

Figure 2.3: Time between samples during acquisition of PPLL Frequency using the SR310 Frequency Counter for 270 seconds of an individual test. These time variations between points correspond to an instantaneous sampling rate that varies from 10 to 40Hz.

The frequency signal was cleaned using a median filter, and any linear system drift was removed based on a curve fit to first reference phase data. Each load phase, consisting of both reference and peak loads was then isolated and average values of PPLL frequency, MTS displacement and MTS Load were taken from the both reference and peak load levels. This data was stored and used to determine peak-peak (p-p) changes during loading.

The main point of interest from the data was the relationship between the PPLL measured frequency and the displacement seen in the phantom. Therefore p-p frequency change was plotted against the p-p change in displacement at each load, and the linear slope and correlation were determined. Note that the relationship truly desired was between displacement changes transverse to loading, along the ultrasound path and the PPLL measured frequency. However due to experimental constraints, these initial tests assumed a

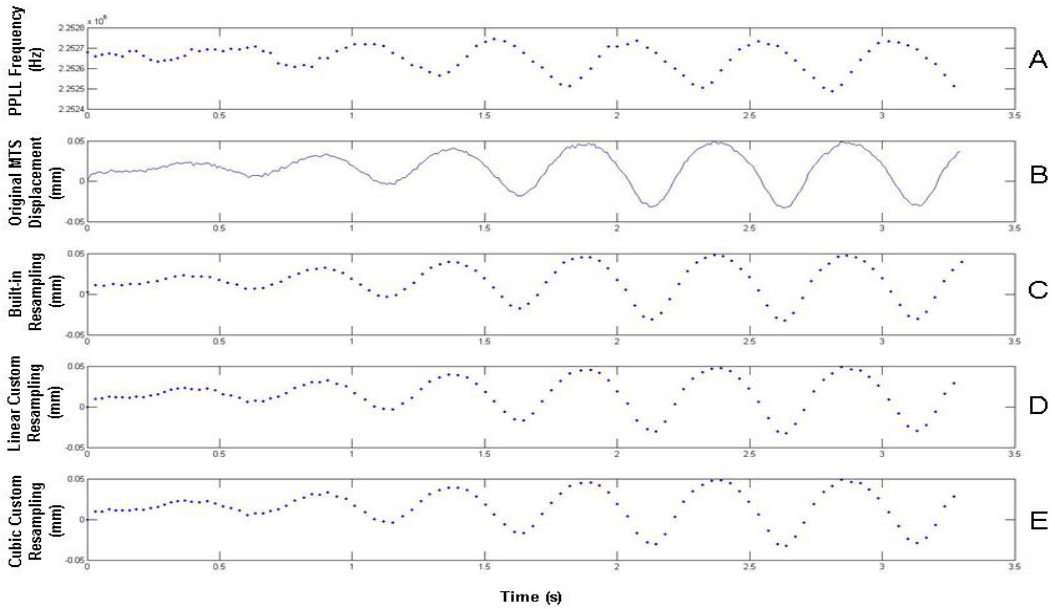

Figure 2.4: Data re-sampling, showing the measured PPLL Frequency during a sinusoidal loading of an extra specimen (A), the measured MTS displacement (B), the re-sampling of the built-in MATLAB 'resample' function (C), the linear custom re-sampling (D) and the cubic custom re-sampling (E). The points in (C) do not directly line up in time with the points in (A), while those in (D) and (E) do.

linear relation between axial displacement in the material and transverse displacement in the material.

The variation seen in this relationship determined whether or not this experimental setup was capable of delivering the measurements desired for non-invasive strain monitoring. The overall variation was reported, as well as the variation when grouped at time points and grouped by orientations to shed light on where the majority of the variation came from.

In order to determine the ability of the PPLL system to predict the experimentally measured values, all the $\Delta f/f$- $\Delta l/l$ data pairs from the 5 flat surface phantom tests are used to fin the best fit curve to the experimental data. Then, this best fit curve is used to calculate the PPLL predicted values of displacement, given a certain level of $\Delta f/f$. Using one load step, from each of the 5 tests on the flat surface phantom, it is possible to determine if the PPLL predicted values of displacement are significantly different from those which were obtained experimentally.

2.3 Results

The flat surface phantom provided excellent results. The average R^2 between MTS piston displacement and corresponding PPLL $\Delta f/f$ at each load level was 0.928 ± 0.032. The average slope of this relationship was 2.63e-4 ± 0.3e-4 mm^{-1}. (Figure 2.6) This showed a variation of approximately 12% in the $\Delta f/f$ - change in displacement relationship over the 5 consecutive tests. This relationship between $\Delta f/f$ and change in displacement was only an approximation between the meaningful relationship of $\Delta f/f$ and $\Delta l/l$ along the ultrasound path. The best-fit relationship to all of the $\Delta f/f$ - $\Delta l/l$ data pairs is actually an exponential

relationship, with an R^2 of 0.8956. (Fig. 2.5) Using this curve, predicted displacement values were found for the each of the $\Delta f / f$ values at the maximum load level. Comparing these predicted displacement values to the experimentally obtained ones, there is no significant difference between these groups, p=0.128. However the power of this test is only 0.219 due to the low sample size of 5.

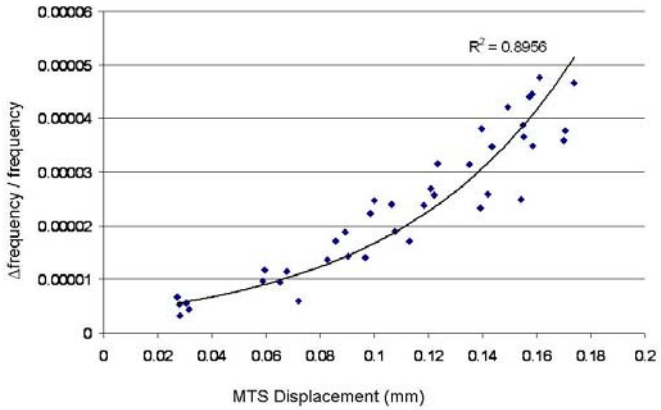

Figure 2.5: Best-fit curve to PPLL-MTS variable data pairs. This Curve is used to find PPLL predicted values of MTS displacement, which are compared to experimentally measured values.

The overall R^2 values for all tests run on the two cylindrical phantoms were found by averaging individual test R^2 values. Using the p-p PPLL frequency change over the reference level frequency ($\Delta f/f$) and comparing them to the p-p displacement change during the applied static loads, the overall average R^2 for the solid and hollow phantoms were 0.89 ± 0.21 and 0.54 ± 0.31, respectively. Grouping consecutive tests without modifying sample position yielded information about dependence on sample consistency. For example, the average R^2 values for Round 1 are 0.97 ± 0.04 and 0.74 ± 0.18 for the solid and hollow phantoms respectively. While for Round 2, the average R^2 values are 0.81 ± 27 and 0.34 ± 0.28. The average R^2 and slopes for each of the 8 data groups described in the methods are reported in Table 2.2, with raw data plots in Figure 2.7.

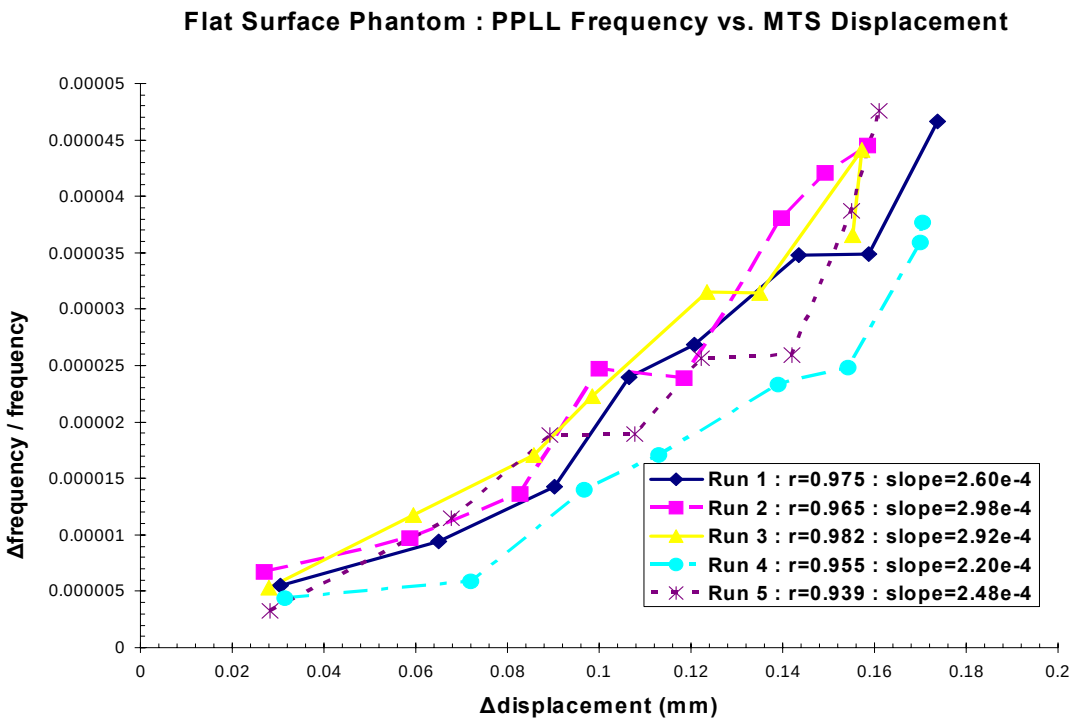

Figure 2.6: PPLL Frequency vs. MTS Displacement relationships for each of the 5 tests on the flat surface, solid phantom.

Group	R^2	Slope [mm]
S.1.1	0.96 ± 0.06	-2901 ± 583
S.1.2	0.99 ± 0.01	-1826 ± 148
S.2.1	0.73 ± 0.39	-1804 ± 195
S.2.2	0.89 ± 0.10	-1690 ± 418
H.1.1	0.76 ± 0.17	-2148 ± 475
H.1.2	0.72 ± 0.20	-2405 ± 982
H.2.1	0.54 ± 0.19	-2175 ± 641
H.2.2	0.14 ± 0.21	-87 ± 1017

Table 2.2: R^2 values and slopes grouped by consecutive tests, describing the PPLL Frequency vs. the MTS Piston Displacement relationship. Slopes here are the displacement over Δfrequency/frequency unit-less variable in millimeters, and theoretically provide a curve for determining the displacement based on changes seen with the PPLL.

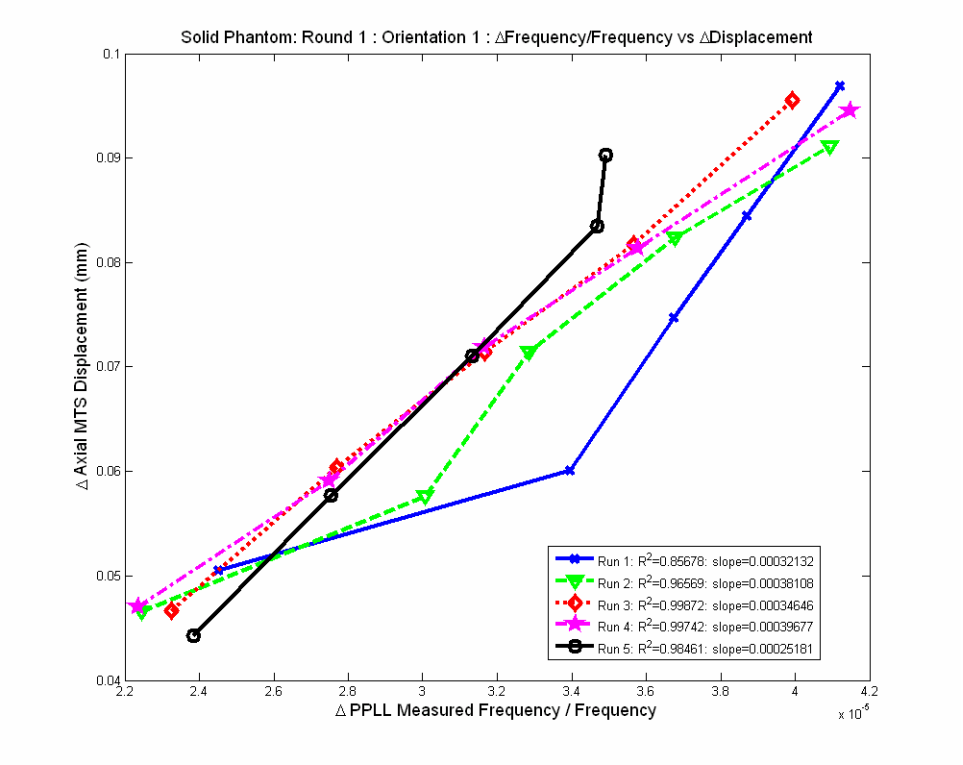

[Figure 2.7.A]

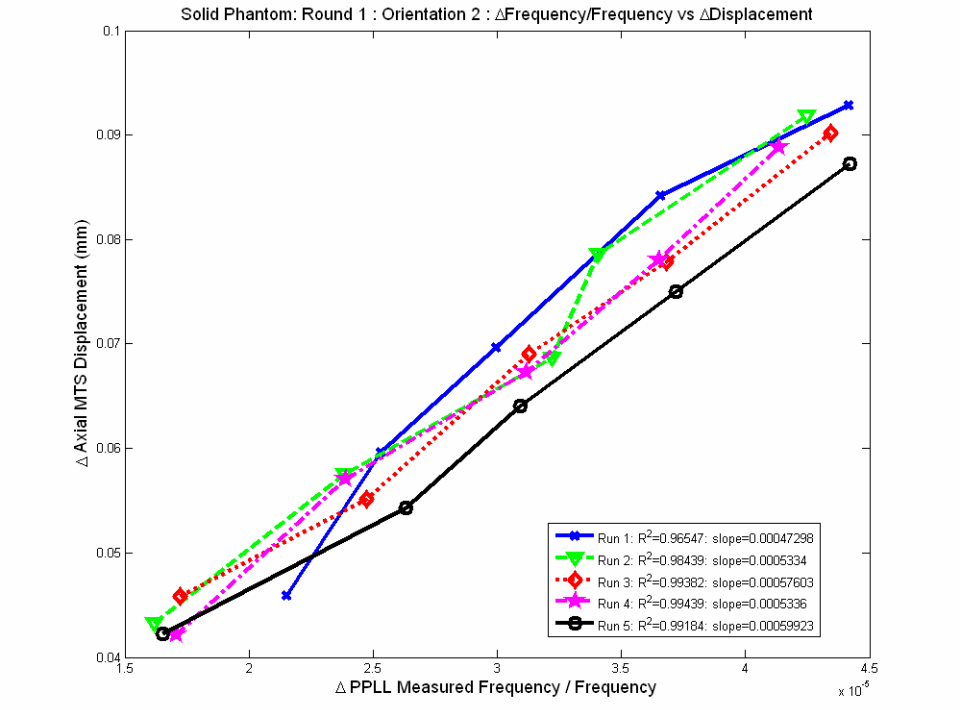

[Figure 2.7.B]

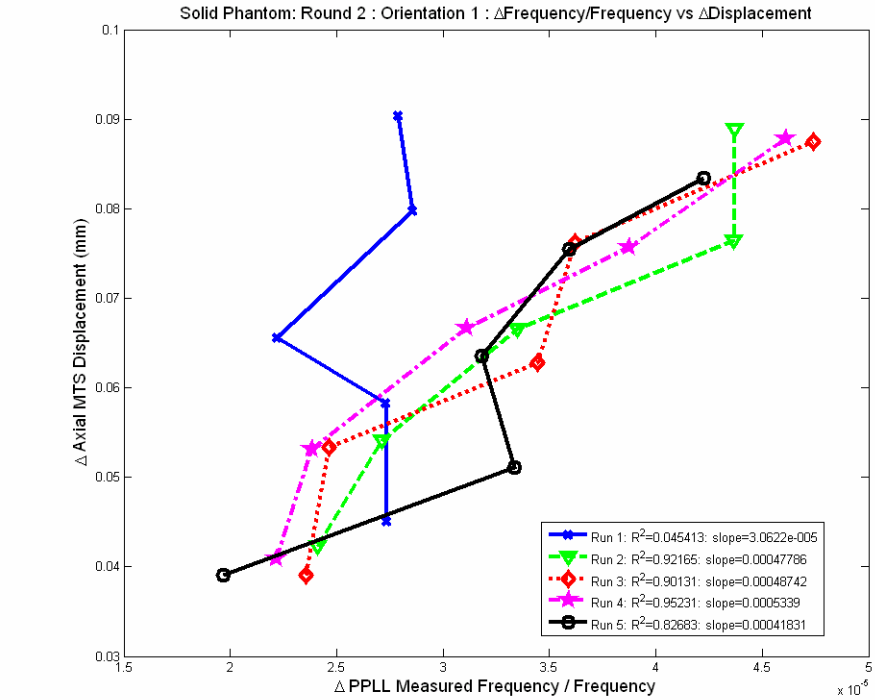

[Figure 2.7.C]

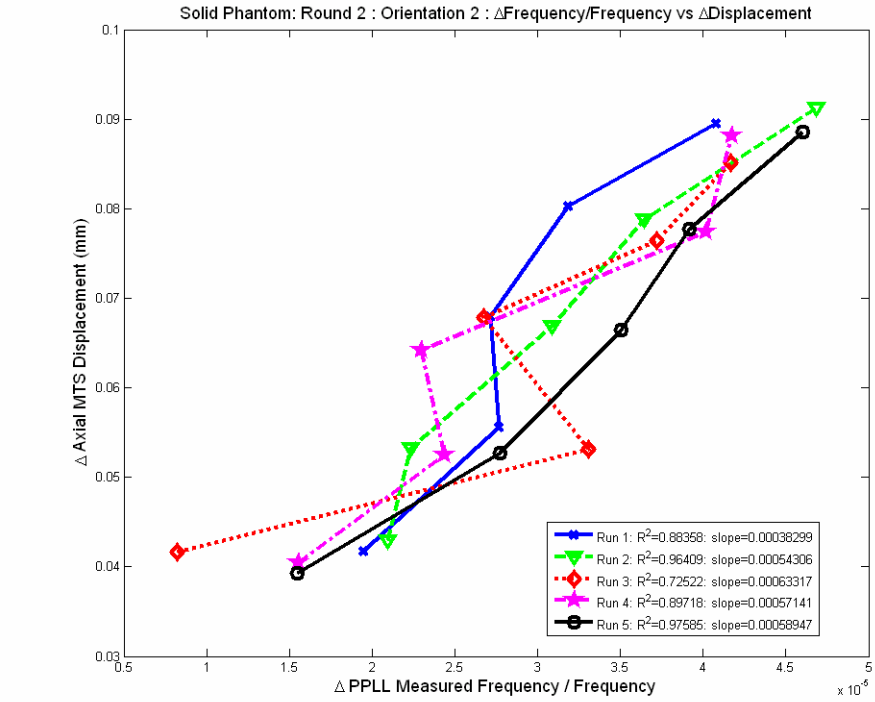

[Figure 2.7.D]

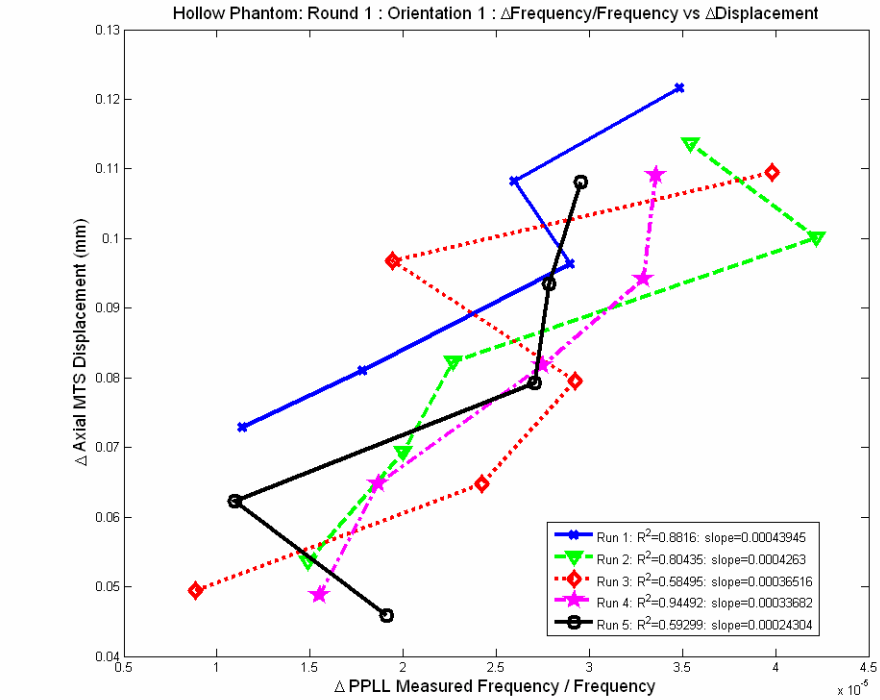

[Figure 2.7.E]

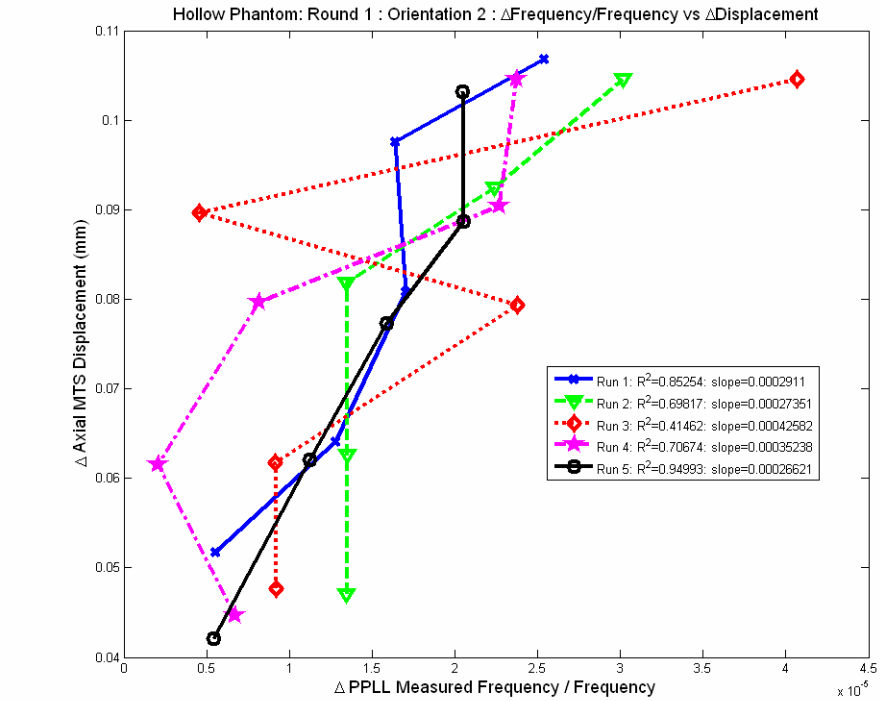

[Figure 2.7.F]

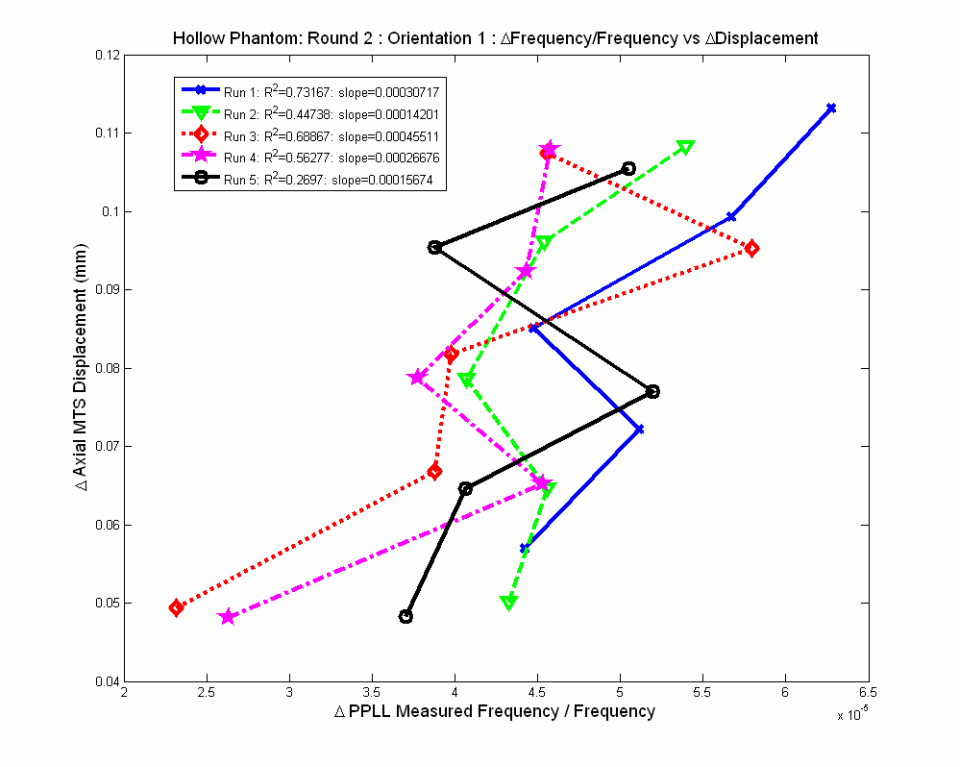

[Figure 2.7.G]

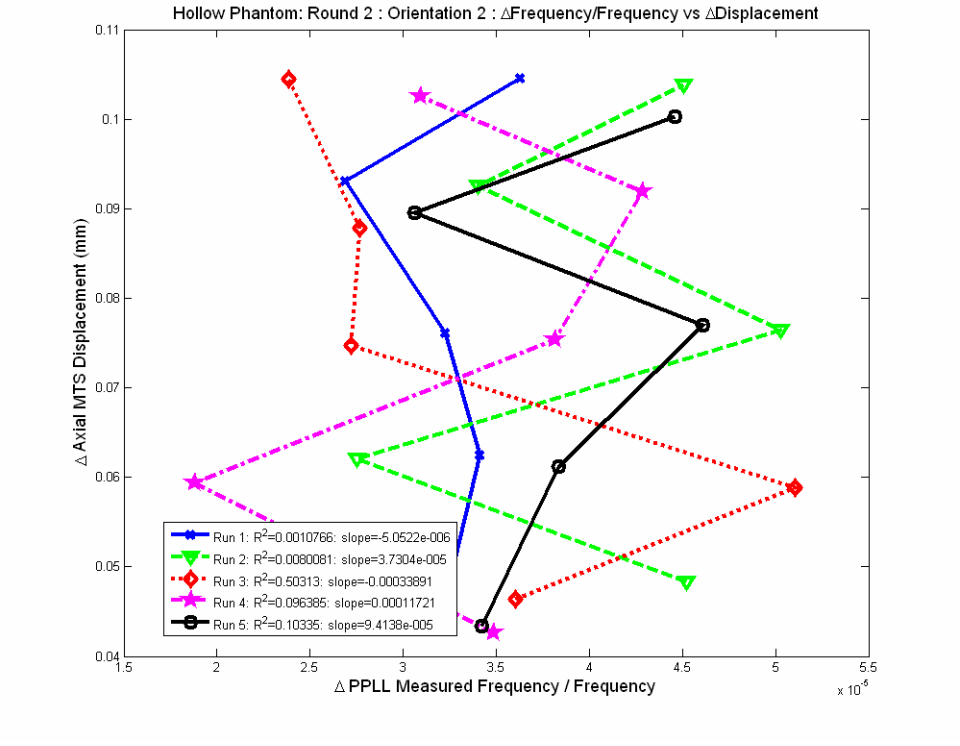

[Figure 2.7.H]

Figure 2.7: Cylindrical phantom raw data and plots of PPLL frequency vs. MTS Displacement, with R^2 values, and slopes in legends. Plots A-D are raw data from the solid cylindrical phantom. Plots E-H are raw data from the hollow cylindrical phantom.

2.4 Discussion

The current research aimed to utilize the PPLL technique to monitor changes in bone phantom material during loading. The overall system performance was good, and provided promising results for the expansion of this technology to bone. Here a new experimental setup was tested for the feasibility of testing bone in-vitro. With an average R^2 of 0.928±0.032 in the flat surface phantom there is a strong relationship between the PPLL measurements and the MTS measurements during loading. Using all the experimental data to obtain the best fit curve for the flat surface phantom data, PPLL predicted values of MTS displacement were found. It was seen that the PPLL predicted values of MTS displacement were not significantly different from experimental values, however this test only lends statistical argument to the already drawn conclusion of a strong relation between PPLL frequency and MTS measurement. The power is to low to determine that the populations are in fact the same, and thus, we can only say that they are not significantly different. The correlation suffers however, as the geometry of the sample becomes more complex. This was to be expected as, the more complex the geometry, the more complex the ultrasound wave propagation, and the more chances for signal interference, scattering, and other possible sources of phase error.

The drop in the R^2 to 0.89 ± 0.21 for the solid cylindrical phantoms yields information as to the setup of the current technology. It is important to note here, that the tests were indeed run in an identical fashion, and theoretically, all slopes corresponding to the PPLL-MTS Displacement relationship should be constant. The fact that the 20 tests on the cylindrical phantom were broken up into groups of consecutive tests provides an understanding as to how sample placement can affect the test outcome. While orientations were kept constant, the movement of the sample in any direction will change the acoustic scatter field, yielding slightly different received waveforms. For example, the acoustic wave may refract at a slightly different angle during propagation. This can result in a different PPLL-Displacement relationship, increasing the variability between tests.

This also allows the consideration of the implications on future calibration issues in a final system design. Based on current results, an external or phantom calibration is not good enough to determine the relationship between the PPLL frequency and any load-dependent variables. The current setup relies on peak-to-peak analysis to determine a PPLL frequency change, and any change in object geometry or placement in the acoustic field will have an impact on this peak-to-peak change. Thus, PPLL changes must be considered to be unique to the precise setup at the time of measurement.

The effect of geometry is even more apparent in the hollow cylindrical phantom. The hollow phantom was used because it has geometry much closer to that of the cortical shell in long bones. The average R^2 value of 0.54 ± 0.31 seen in all the hollow phantom tests shows a drastic reduction in PPLL correlation to the MTS piston displacement, a load dependent variable. While the tests were run in the exact same manner as the solid phantom, the apparent performance of the PPLL system is drastically reduced, pointing toward the effect of the complex sample geometry on the acoustic field propagation. This is vital to the understanding of what the PPLL is in fact measuring. If propagation follows the “straight line” path between the transducers, then phase interference issues arise with the signal reflection inside the cortical shell. If there are too many cycles in the burst, the front edge will reflect inside the shell, and create interference with the tail end of the signal. Then

depending on where the lock-point is chosen, this interference may have a large effect on the phase comparison, and hence PPLL measurement.

A main concern for the current testing was the decrease in performance as the sample was tested repeatedly. This brings into question of whether or not the material itself was in fact changing during loading, possibly causing some of the experimental variability. It can be noted on the MTS Displacement vs. PPLL Frequency graphs that the maximum displacement due to the 800N does not shift too much during the testing, however it is curious that the slope of the MTS-PPLL relationship steadily declined as the testing progressed. If the material properties were changing as testing went on, then the acoustic propagation speed also changed, and thus the P-P change in frequency was also affected. In the future, it would be interesting to determine how well the PPLL tracks the load-displacement curve when loading a sample to failure. This may also provide some interesting information on post-failure material properties and resulting phase comparisons.

Chapter 3: PPLL Technique Sensitivity to Compressive Loading in Bone Tissue

3.1 Introduction and Rationale

The current research is not only applicable to the biomechanics research field, but also to disease diagnostics. The application in osteoporosis alone has widespread implications for this research, and thus the goal is to begin work utilizing Pulsed Phase-Lock-Loop technology in the ultrasonic probing of bone material during loading. Previous work suggests the tracking of intracranial pressure can be done with the PPLL by tracking the extremely small variations in cranial diameter due to internal pressure. Here, we are look at changes of the femur bone encasing the marrow cavity (compared to the skull, with the brain cavity). In this case it may in fact be pertinent what material exists inside the cavity. Since any increase in bone dimension along the 'straight-line' ultrasound path must mean a decrease in "fluid" dimension along that path, the fluid in question may have an effect on overall percent time-of-flight velocity change. Considering marrow is predominantly fatty tissue, the acoustic velocity will actually be slightly less than in water, so an increase in bone dimension will cause a greater percent velocity change is the "fluid" dimension consists of marrow, instead of water. To test the importance of this, two groups will be utilized, one group with the marrow left intact, and one group with water filling the marrow cavity.

The previous chapter demonstrated this PPLL technology is sensitive enough to measure changes in phantom material, with more simple geometries. Continuing on with the overall objective of this work, to utilize PPLL technology in applications for bone tissue, the second specific aim of this research is to show the PPLL responses seen during loading of bone material. This work will show if the PPLL technique can be used to detect changes in bone during mechanical loading, and that the marrow inside the marrow cavity will provide better responses due to its decrease speed of sound.

3.2 Experimental Setup

To successfully complete our objective, the PPLL system provided by Luna Innovations was used in monitoring bone samples during loading by a MTS axial load frame. The bone samples used in this research were taken from sheep femurs based on their availability and size. The sheep femurs were monitored with the PPLL technique during mechanical loading to verify that the system is capable of detecting finite changes in biological material.

Cortical Shell Preparation:

Fourteen bone samples were taken from fresh frozen sheep femurs. The samples were cut to approximately 6cm in length at the mid-diaphysis. The bone samples were split into two groups. The first group (Group M, N=10) was tested with the bone marrow left intact. The second group (Group W, N=10) was tested with the bone marrow flushed out of the cavity with a water-pick, and filled with de-gassed water. Of the 14 bone samples used, 10 of those were tested with the bone marrow intact. Six from the intact bone marrow group, and four additional samples were cleaned of marrow and tested again, yielding 10 bones tested with only water inside the marrow cavity. Within each group, each of the 10 samples was tested in 3 orientations. These tests were treated independently due to varying bone geometry along the ultrasound path for each test. This yielded a total number of 30 tests per

group. The three orientations were similar across bones, taking each orientation to pass roughly through the area above its respectively numbered strain gauge. Strain gauge one was always placed on the anterior surface of the cortical shell. Strain gauges two and three were then distributed equally around the circumference, in a counter clock-wise direction looking down the femur axis.

Mechanical Loading Protocol:

Loads were kept well within the elastic regions of the bone samples, with similar load and rest periods as described in chapter 2. As in the case with the cylindrical phantoms, to ensure even load distribution, the contact ends of the cortical shells were embedded in self-curing acrylic. Briefly, the static loads were applied with a MTS Minibionix 858 (MTS Corporation, Minneapolis, MN) axial load frame with their TestStar II control software. The static loading protocol began with a 50N preload to ensure solid contact between the piston and sample. The loading protocol then consisted of 8 load phases, of 100N – 800N with 100N steps for a length of 16 seconds. Each load phase was separated with a 16 second reference phase where the load was held at 50N. Due to system drift and the large time scales used in the static loading procedure, the analysis was done on a peak-to-peak (P-P) basis using the adjacent reference loads as points of comparison to the load phase, as opposed to using the initial 50N preload level. The sample was loaded with the MTS in the axial direction of the cylinder, while the ultrasound transducers were held in the water bath transverse to the axial direction. Therefore, any dimensional change investigated by the PPLL would be in the transverse direction to loading, and a result of material expansion during compression.

System Setup:

The test setup was almost identical to the setup for the phantom material experiments. The same PPLL system built by Luna Innovations, Inc. was used. This system has two 0.5 inch diameter immersion transducers with a central frequency of 2.25MHz. While the wavelength depends greatly on the assumed sound velocity, the literature estimates roughly 1500m/s and 3600m/s for acoustic velocity and thus a wavelength of roughly 0.67mm and 1.6mm in water and bone respectively. The transmitting transducer was focused with a focal length of 0.5 inches. The receiving transducer was a plane transducer. The bones were each tested under the same setup as the phantoms, and can be seen in Figure 2.3. Briefly, this setup consisted of the sample and transducers inside a small bath containing de-gassed water for acoustic coupling. The acoustic signal was supplied by the PPLL was sent through the sample, then collected and passed through an amplifier and then split between the PPLL and an oscilloscope. The variable frequency PPLL device sent a reference signal to a frequency counter for data acquisition. In addition to the PPLL and MTS variables, strain gauges were used to determine local strain fields. Therefore the LabView control panels for the PPLL were modified. The PPLL control was left to the LabView program supplied by Luna Innovations, while data acquisition was removed from it, and combined into a separate LabView program which controlled data acquisition from both the PPLL frequency counter, and the National Instruments Strain acquisition box, model SXCI 1541. This acquisition program contained a software trigger, which was hooked up to an external push button switch. This switch was used to ensure the data acquisition for both the MTS variables and the strain and PPLL variables began simultaneously.

The data acquired for each test includes; (1) the frequency from the PPLL, (2) the strain from the rosette strain gauges attached to the bone surface, and (3) the load, and piston

displacement from the MTS. A Dell Laptop was used to run the PPLL control program, as well as the acquisition program for the PPLL frequency and the strain. The strain and trigger voltage signals entered the custom acquisition program through a National Instruments DAQCard 6036E PCIe card, while the PPLL frequency was only attainable through ActiveX controls provided by the frequency counter manufacturer (Signal Recovery, Model SR3280).

Data Analysis:

Simple static loading was used to determine how well the PPLL technique could correlate to local strain in bones. At each of the 8 static loads, the load, MTS piston displacement, local axial strain, local circumferential strain and PPLL measured frequency an average value for the duration of the static load was found. The average values were calculated from 3 seconds before and after the step load was applied. This was done due to system drift and low frequency noise that often caused some variation over the entire 16 seconds of load application. Three main correlations were reported: 1. PPLL frequency vs. MTS displacement (P-P ΔDisplacement); 2. PPLL frequency vs. axial strain; and 3. PPLL frequency vs. circumferential strain. The PPLL frequency refers to the unitless quantity of the P-P difference in frequency output divided by the reference level frequency (ΔFrequency/Frequency). MTS displacement was calculated as the P-P difference at each reference-load phase pair. Local axial and circumferential strains were determined using the rosette strain gauge data with the assumption that there was a 2D linear strain field in the plane level with the gauges transverse to the loading axis.

The 2D linear strain field utilizes the planar equation,

$$a*x+b*y+c=\varepsilon$$

where a,b,c are constants, x,y are the coordinates in the plane of the bone cross-section, and ε is the strain at those coordinates. Using the three strain gauges, it then becomes possible to solve for a,b,c by solving the linear system:

$$AX=\varepsilon$$

where A is a matrix of respective gauge positions, $A=\begin{bmatrix} x_1 & y_1 & 1 \\ x_2 & y_2 & 1 \\ x_3 & y_3 & 1 \end{bmatrix}$, X is the column vector of constant coefficients, $X=\begin{bmatrix} a \\ b \\ c \end{bmatrix}$, and ε is the column vector of respective measured strains,

$$\varepsilon=\begin{bmatrix} \varepsilon_1 \\ \varepsilon_2 \\ \varepsilon_3 \end{bmatrix}.[37]$$

Two linear strain fields were calculated for each test: one for axial strain, and the other for circumferential strain. To obtain the axial strain field, the values for ε in the above equations are the axial strain values measured from the 3 rosette strain gauges. For the circumferential strain field, the circumferential strain values from the rosette strain are used for ε. In order to obtain the x,y coordinates of each strain gauge, a tomographic slice of the bone was taken at the gauge level using a vivaCT40 (SCANCO Inc., Switzerland) scanning

at 76μm resolution. The x,y coordinates were taken to be the pixel location at the middle of the strain gauge. Based on recorded PPLL orientations with respect to the bone, x,y coordinates (pixel locations) were also determined for the point at which the ultrasound enters and exits the bone along a straight line path from transmitting transducer to receiving transducer. The average of the inlet and outlet strain was then used in the correlation with the PPLL frequency at the different levels of mechanical load. Since the strain gauges gave surface measurements only, the bone's internal geometry was not taken into account, therefore this method only takes into account the strain at two points along the entire ultrasound path.

In addition to the above comparison, a very rough estimation of the ultrasound path length (ΔL) was attempted using the following assumptions. The main assumption was that the ultrasound path followed a straight line from transmitting transducer to receiving transducer. To estimate ΔL, the same cross-sectional image of the bone was used to determine the original thickness of the cortical shell along the straight line ultrasound path. Then averaging the axial strain calculated for each point in the 2D linear strain field along the straight line ultrasound path, an average axial strain was calculated. This average axial strain was then multiplied by 0.3, a Poison's ratio commonly used for bone. This would give a rough estimate of what the average transverse strain will be along the ultrasound path. Assuming small strains, the basic equation of

$$\varepsilon = \frac{\Delta L}{L}$$

is then used to find ΔL, utilizing the calculated average transverse strain and the original path length found from the bone cross-section. This ΔL was then correlated to PPLL frequency to allow a rough correlation to the physical parameter which is part of the basis of ultrasound TOF measurements changes in the PPLL.

During data acquisition, if any part of the system failed, that test was removed from the correlations affected. For example, if one of the off axis elements of the rosette strain gauges failed, this would only affect the circumferential strain calculations, so it would be removed from the PPLL vs. circumferential strain correlation only. Also, during mechanical loading under force control, occasionally the system would begin to rapidly diverge in its error calculations, especially during step loading. Therefore if the MTS should fail, but more than 5 cycles were completed, the correlations were still completed, except with fewer load phases, thus fewer points in the individual test correlation.

3.3 Results

The correlations between PPLL and calculated strain rely not only on the performance of the PPLL, but also the performance of the functions which calculate the local strain; therefore sample results from those calculations are presented here to demonstrate their efficacy. The local strain calculations were done through MATLAB using a cross-sectional image of the bone taken at the level of the strain gauges. Figure 3.1 shows the parsing of the acquired data, where only 3 seconds on either side of the step load were used for analysis. For the strain values there was no need to compare to reference, as the strain is inherently a change compared to the zero level.

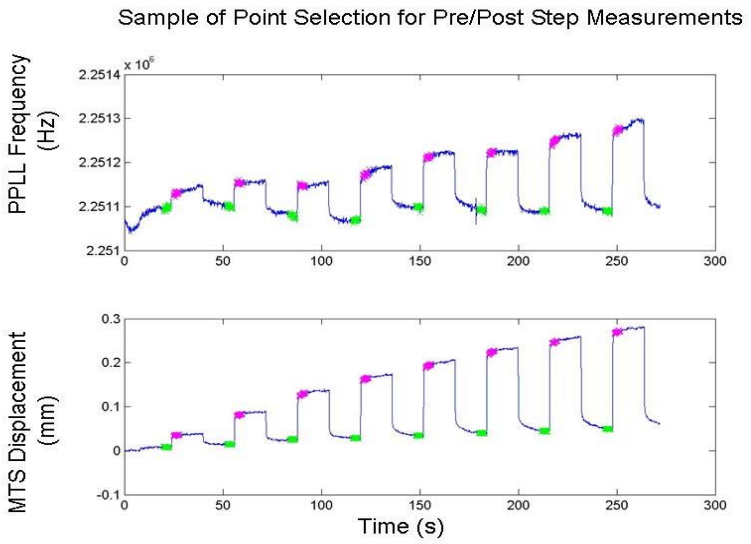

Figure 3.1: Representative plot to show points selected to compute the average static load. The green dots (dots just before the step load) are the points taken from the reference level, while the pink dots (dots just after the step) are from the load level. This sample plot was taken from Bone 2 Orientation 3. Top graph is PPLL Frequency vs. Time. Bottom graph is MTS Displacement vs. Time. The same time points were used from 9 strain gauge channels.

Each load level in each test had an associated PPLL frequency, MTS displacement, and strain measurement from each of the 3 rosette gauge elements. These 9 strain measurements were translated into axial and circumferential strain measurements at the point of each strain gauge by calculating the 2D linear strain field as described above. An example of this 2D linear strain field can be seen in Figure 3.2, where any pixel on the bone is given a strain value according to the calculated strain field, and all off-bone pixels are given a value of zero. The average amount of axial and circumferential strain at the surface point of entry and exit was correlated to the measured PPLL frequency.

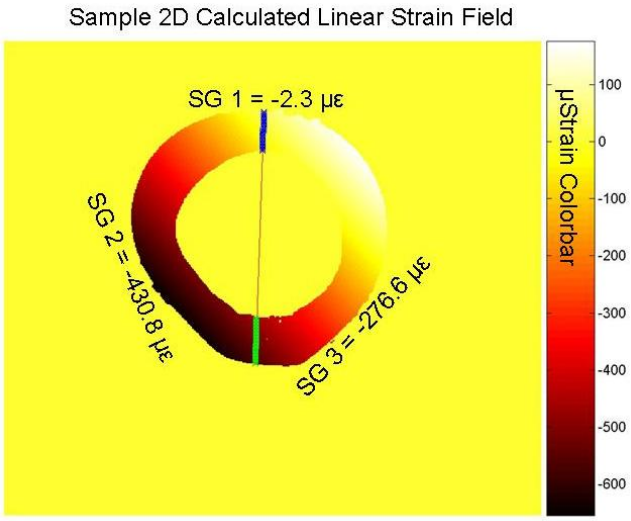

Figure 3.2: Sample 2D calculated linear strain field. Strain field calculation uses 2D cross-section of bone geometry obtained via μCT scanning at 76 μm resolution. Line indicates "Straight line" ultrasound path in current orientation. Strain gauges are located on the bone surface closest to their labels (SG 1-3), and have the given measured value of axial strain. This sample was taken from Bone 2, Orientation 1 under the maximum 800N load.

Due to the varying geometry across bones, and across individual orientations within bones, the tests were grouped by their intramedullary cavity contents; Marrow or Water. Each of the PPLL frequencies were correlated to MTS displacement, calculated axial strain, calculated circumferential strain and, the estimated change in ultrasound path length through bone, as shown in figure 3.3. The average R^2 values between PPLL frequency and MTS displacement was 0.71±0.28, and 0.60±0.32 for group M(n=30) and group W(n=26) respectively. The average R^2 between PPLL frequency and locally calculated axial strain is 0.70±0.27, and 0.62±0.29 for groups M(n=29) and W(n=24) respectively. For PPLL frequency vs. locally calculated circumferential strain, the average R^2 values are 0.61±0.29, and 0.65±0.30 for groups M(n=29) and W(n=21) respectively. Using the rough estimation of ΔL, the R^2 values between PPLL frequency and ΔL are 0.70±0.27, and 0.63±0.28 for groups M(n=29) and W(n=24), respectively. All groups with less than n=30 have samples removed due to experimental system failure, such as the strain system, as described in the last paragraph under data analysis. While there seems to be a trend of better correlations with marrow rather than water supporting the idea of a higher TOF percent change due to lower "fluid" sound velocity, no statistical significance could be found between the marrow and water groups for any of the relationships given above. This is attributed to the high variation, and non-normality of the data.

The expected relationships were not always obtained. In fact, the data are not normally distributed about the mean, as seen in the histograms (Figure 3.4). There were tests that performed very well, with R^2 values above 0.95, while there were tests that performed poorly with R^2 values of less than 0.05.

The raw data was reviewed for possible explanations. In many tests there was either none, or very little, PPLL system response to loading. In several tests, the PPLL showed a response to loading, however the change in frequency was opposite to that of what was expected, causing the relationships to MTS displacement, axial strain, and circumferential strain to be inverted. This could be due to many reasons, including poor lock-point selection and excessive noise, which are left to the discussion. Samples of highly correlated, no PPLL response, poor correlation, and inverted PPLL response are shown in Figure 3.5. Under current experimental protocol, no further testing was done.

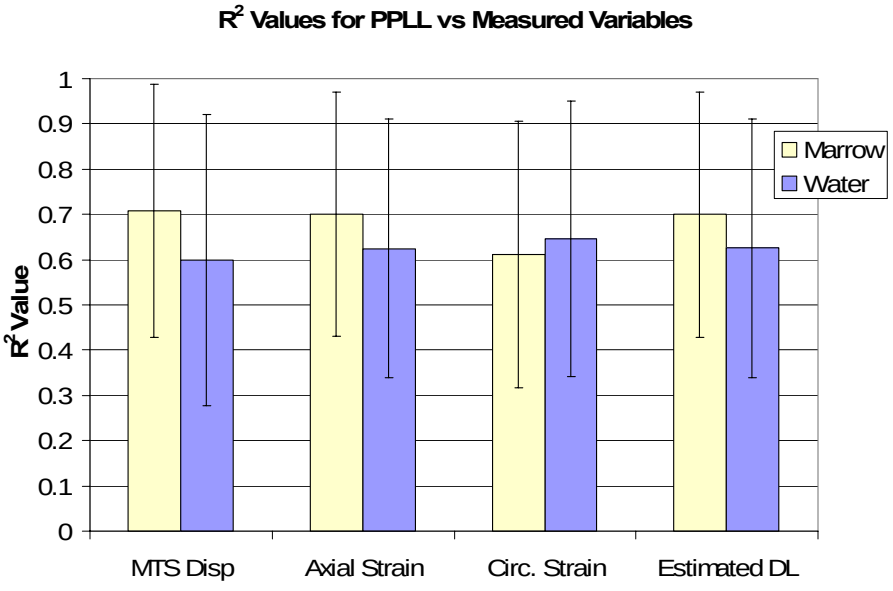

Figure 3.3: Mean ± Standard Deviation of R^2 values for PPLL frequency measurements correlated to given measured or calculated variables.

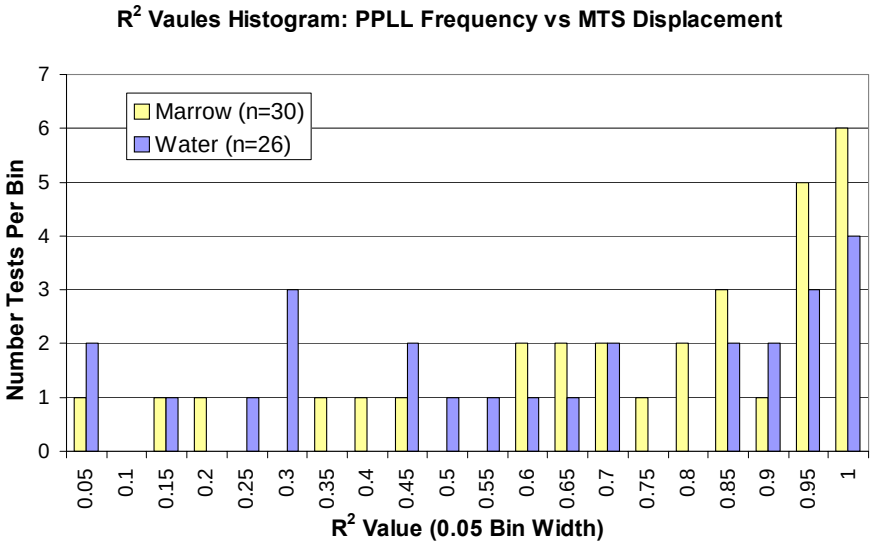

[Figure 3.4.A]

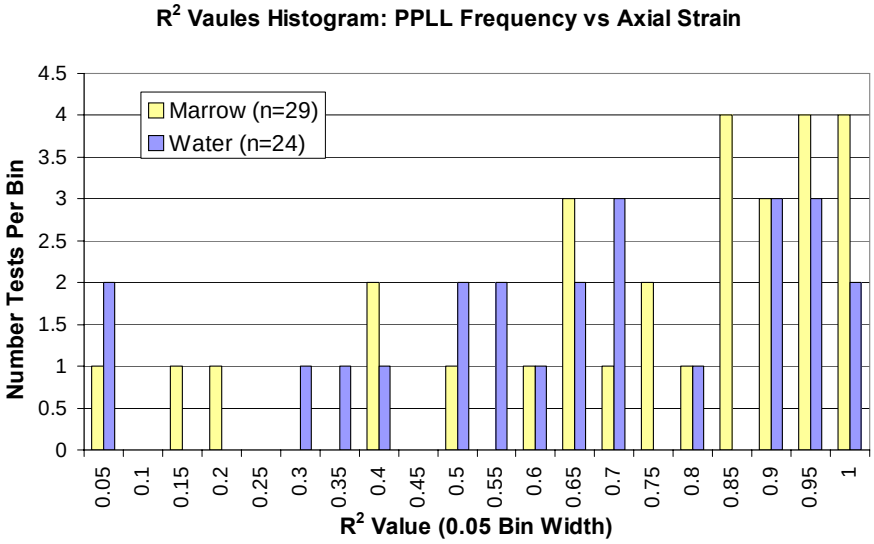

[Figure 3.4.B]

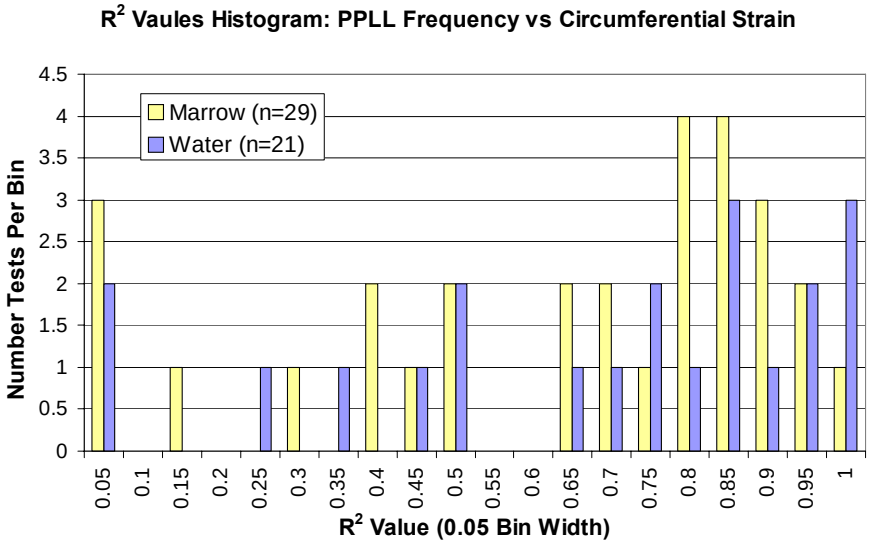

[Figure 3.4.C]

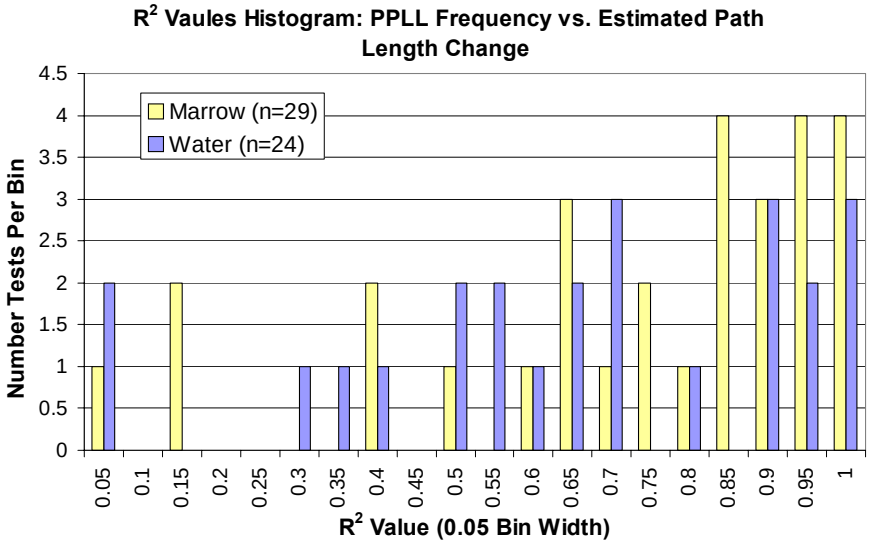

[Figure 3.4.D]

Figure 3.4: Histograms of R^2 values for PPLL Frequency vs. Measured Variable Correlations. A) PPLL vs. MTS Displacement, B) PPLL vs. Calculated Axial Strain from 2D Strain Field, C) Calculated Circumferential Strain from 2D Strain Field, D) PPLL vs. Estimated Change in Ultrasound Path Length using 2D Strain Field

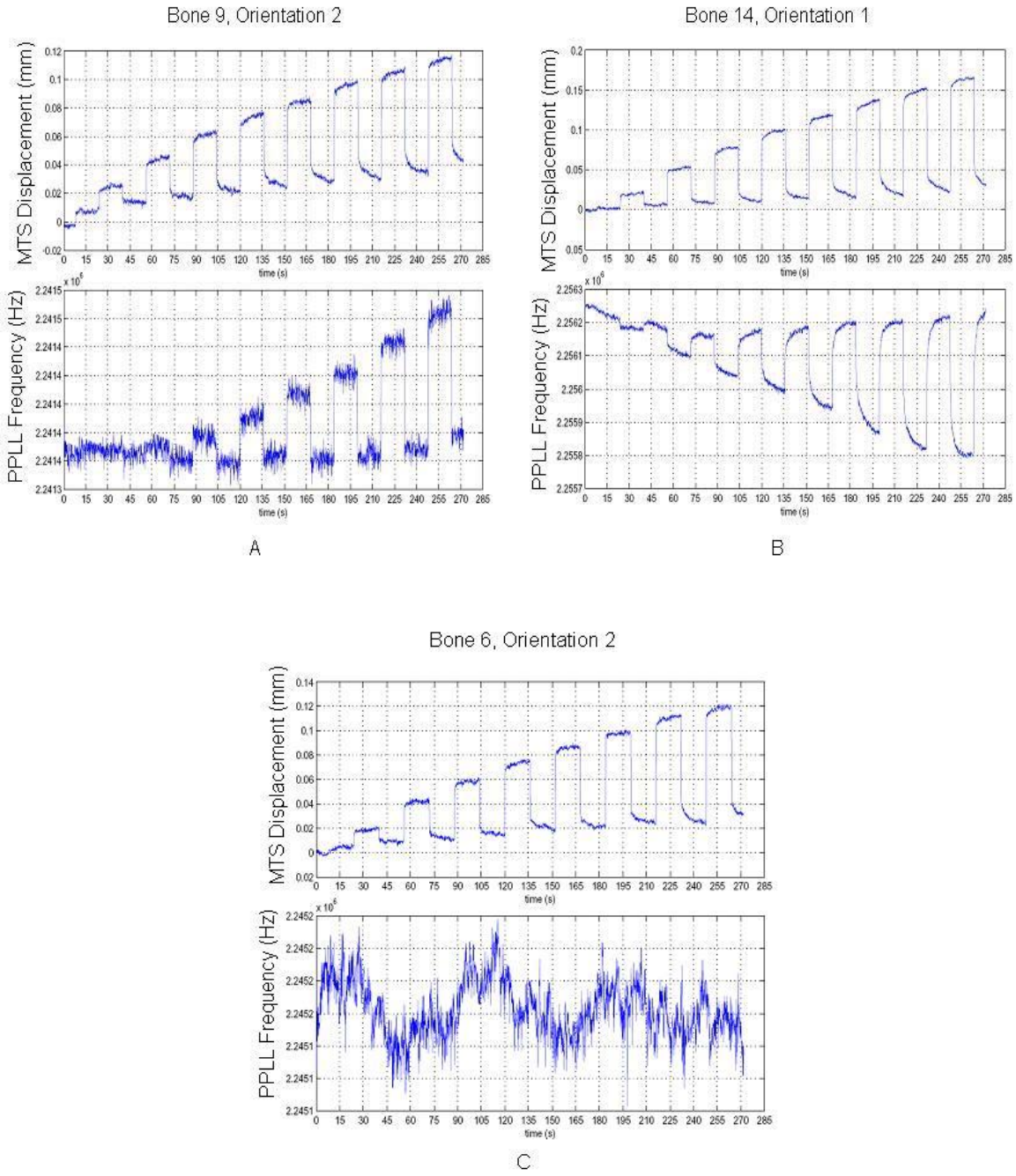

Figure 3.5: Raw data of both MTS displacement and PPLL frequency, vs. test time. A) Bone 9, Orientation 2 shows strong expected relation, with correlation constant of -0.991. B) Bone 14, Orientation 1 shows strong unexpected relations, with correlation constant of 0.996. C) Bone 6, Orientation 2 shows no PPLL response to loading, with a correlation constant of 0.512. The correlation constants above are all for PPLL Frequency vs. Calculated Axial strain, which as the axial strain gets more negative (higher compression), the frequency is expected to increase, yielding a negative correlation.

3.4 Discussion

The goal of this research was to demonstrate the ability the Pulsed-Phase-Locked-Loop (PPLL) technique, which has shown good response to detecting changes while loading; however the experimental setup must be modified to reduce variability before use as a practical application. There are several known contributors to the high variability; however they do not explain the instances where the PPLL simply did not respond. In these cases only speculative causes can be made for possible future testing.

The overall system performance has shown that there is some relation between the PPLL measured variables and the local strain environment. The uneven distribution of performance, with several very highly correlated results, shows that the PPLL measured variables are in fact very closely related to the local mechanical environment under ideal circumstances, and may in the future be used to predict strain. There are several sources of possible variability in the experimental protocol, which includes ultrasound and geometric considerations, as well as PPLL system considerations.

Given the complex geometry of bone, the ultrasound path through the sample might be more complicated than the originally predicted "straight line of flight." During data processing local strain environments were taken at the inlet and outlet points of the straight path between the two transducers. Given the fact that the estimation of ΔL did not correlate any better than taking the average strain, ignoring the inner bone dimensions, it can be concluded that this "straight-line" path assumption is invalid. The determination of the true ΔL is complicated by other possible ultrasound paths through the bone. One possible path is that the ultrasound may follow the cortical shell around its circumference. Given that the speed in bone is about twice that of water (and marrow), if the path length through the cortical shell circumference, which strictly consists of bone, is more than twice the length of the diameter of the marrow cavity, the first ultrasound energy picked up will not follow the "straight line" path. Furthermore, if the all bone path is very close to twice the straight path, then the ultrasound energies traveling along the two different paths will actually interfere with each other, causing artificial

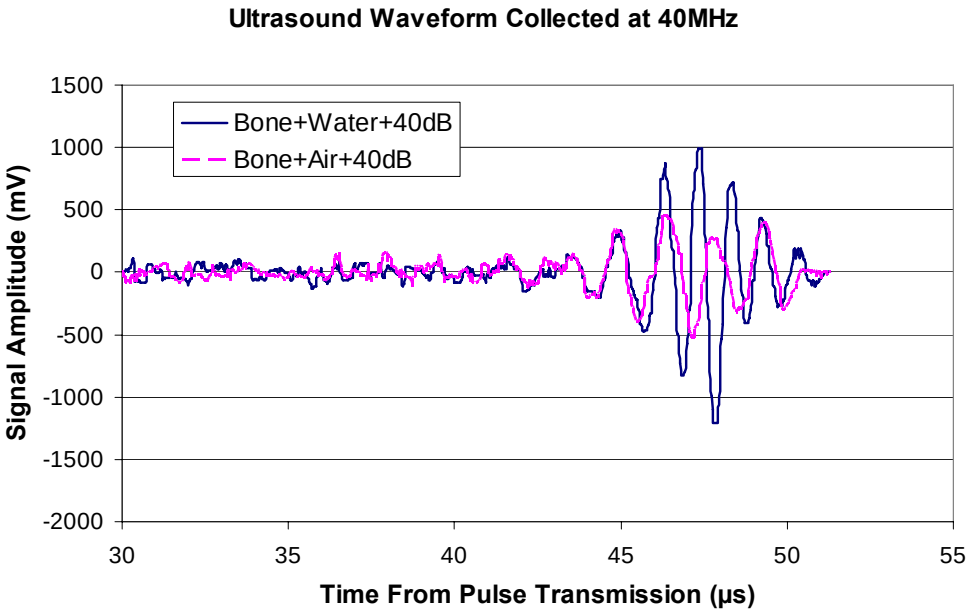

Figure 3.6: Raw ultrasound waveform collected at 40MHz. First signal has water inside the marrow cavity to allow through transmission (blue). Second signal has air in marrow cavity, allowing only transmission through cortical shell (purple).

phase shifts that will throw PPLL measurements off. Performing a simple waveform acquisition with water and air in the inner marrow cavity showed that the signal received can indeed be a superposition of the signals from the different paths. The waveforms acquired (Figure 3.6) with air inside the marrow cavity showed that even when no ultrasound can penetrate through the marrow cavity; it is still possible to receive a detectable signal. More importantly it shows that this signal arrived at very close to the same time as the signal with water present in the marrow cavity. This means that the received signal in the previous experiments are a combination of the two signals, and since they travel through different media, and one undergoes reflection and refraction at the two endosteal surfaces, the two signals will have different phase. The superposition of these two signals results in a phase shift of the received signal that is not related to the desired measurements, and therefore gives rise to a large source of error. Future work will have to ensure a known ultrasound path to be able to precisely determine the change in path length detected by the PPLL.

Another complexity arising from the geometry of the bone is the dissipation of wave energy, resulting in noisy received signals. The multiple reflective surfaces (the total number depends on the path taken) attenuate energy from the signal. With this attenuated energy and the receiving transducer setup used, only a small portion of transmitted energy can be expected. Future setups using the PPLL technique may get around both the ultrasound path and the attenuated energy problems by utilizing different transducer setup, such as pulse-echo mode tracking the expansion of a single shell only. It is possible to transmit and receive from the same transducer. This pulse-echo technique may prove more reliable in the future.

Within the PPLL controller there are several tunable variables which might provide more consistent results. The cycle number, for example, can shorten or lengthen the ultrasound bursts in space. This would provide slight changes in wave energy propagation, especially in thin reflective media, such as the cortical shell. In the experimental setup used, the system was used as delivered, with controller software that removed these controls. It is noted that with 15 cycles of a 2.25MHz sinusoid, the approximate burst width in bone at 3000 m/s is 18mm. Thus within the cortical shell, the beginning few cycles of the waveform can reflect off the endosteal surface and then the periosteal surface before the last few cycles enter the bone. At that point, the beginning of the burst would interfere with the end of the burst. This interference can be alleviated by either changing the cycle number to ensure it does not occur, or by choosing a system lock point somewhere in the middle of the burst, before the interference starts. With the current setup, it was difficult to determine where in the burst to set the lockpoint, therefore, future tests should be done with fewer cycles, or with the pulse-echo method to ensure no interference.

Given that biological variability is random, and measurement error is random, it is curious to find results which are not uniformly distributed. This means that on top of measurement errors due to complex ultrasound paths, either the errors are multiplicative, or there is another source of error which contributes to the non-normality of the data. When looking at the strain fields calculated it can be seen that the bone can be in both tension and compression during these tests, due to bending. The compressibility of bone leads to altered local densities at sites of tension and compression. Since the speed of sound depends on $\rho^{-1/2}$, the density changes can contribute to the velocity changes seen in the PPLL measurements. Combining the possibility of multiple paths, with the fact that if areas of tension and compression exist along the ultrasound path they can effectively cancel each others effects on

velocity, it can bee seen that it is possible to get some tests with little to no PPLL response. This can lead to the non-normality of the data.

Experimentally minimizing both the ultrasound path and the reflective interference problems should drastically improve the repeatability of these tests. The system has proven to be useful in many other applications [14, 17, 19, 21, 22], and can be consistent in phantom material, as shown in chapter 2. It has also been shown, in other research done in our lab, to be fairly consistent when scanning and loading the whole calcaneus. This lends itself to reduced path and interference problems by the different natural geometry of the sample. Additionally, using the PPLL technique along the loading axis by taking advantage of the surface waves and angled transducers may be more useful. The work here has shown the PPLL technique is capable of detecting minute changes in bone during loading, and future work should be done to explore alternate experimental setups for specific purposes.

Chapter 4: PPLL Measurements Compared to Geometric Changes Seen in Finite Element Models

4.1 Introduction and Rationale

In the previous chapters, the PPLL technique has been shown to be sensitive to changes in both phantom and bone during mechanical loading. However in the previous chapters no relationship was able to be determined between the PPLL measured variable (VCO frequency) and the change in bone dimension along the assumed 'straight line' ultrasound path. Due to technical loading constraints, it was not possible to load and collect ultrasound measurements along the same axis. Therefore, while the correlations in the previous chapters to axial direction variables is good, these variables do not tell the full story of mechanical environment seen in the direction of ultrasound penetration. Using finite element models of each bone geometry it will be possible to extract strain parameters along the three main propagation paths of ultrasound energy; straight through, and around the cortical shell in both right and left directions. This should yield overall path length changes seen by the ultrasound, and should thus be more precisely related to the PPLL measurements. Using the path length changes from the FE model, and the PPLL measurements it should be possible to obtain a relationship between $\Delta l/l$ and $\Delta f/f$. This relationship should be constant across bones and geometries, so long as the main physical phenomenon measured by the PPLL is changes in dimension. If this relationship varies more than expected across bones, it may be a sign that not only change in dimension, but also change in material property during loading must be taken into account when using PPLL measurements.

Utilizing the Finite element method may also help to dispel some of the variation seen in previous chapters. By using the cross-sectional geometries, and estimating ultrasound velocities and paths, it may be possible to estimate whether or not the interference and ultrasound path issues discussed in the previous sections do in fact contribute to phase error. It may even be possible to estimate the size of these errors, thus allowing conclusions to be drawn about the importance of minimizing these effects in future testing.

There are two main objectives of the finite element modeling work. The first is to use nodal displacement information to determine ultrasound path length changes along the three main possible propagation paths, and correlate these path length changes to the PPLL frequency measurements. This will be done by creating an individual FE model for each bone geometry, and using linear-elastic approximations over the entire range of load. The second objective is to use the linear-elastic models to step-wise approximate the non-linear nature of the bone to theoretically determine the presence of phase artifacts due to signal superposition of the three main propagation paths. These step-wise nonlinear approximation models can also be used in the same comparisons to PPLL frequency to determine if relationships to PPLL frequency can be strengthened over previous load-variable comparisons.

4.2 Experimental Setup

FE Model Geometry, Materials and Properties

In this application, finite element modeling will be a useful tool in describing geometric changes during loading that would otherwise unobtainable. Given the fact that we are using sheep cortical shells from the mid-diaphysis, the models will make the basic simplifying assumption of linear elastic material properties. While cortical bone is generally

thought of as orthotropic in its material properties, the models will assume an isotropic material. Isotropic, linear-elastic material properties are widely used in the literature for cortical bone, and since our application is not a material evaluation or failure prediction, but rather a simple extraction of geometric parameters, these material properties will provide adequate results. The geometry for the models will come from each individual bone, scanned in a micro-computed tomography scanner (vivaCT40, SCANCO Inc., Switzerland). The spatial resolution of the microCT scanner used to obtain bone geometry was set to 76 microns. While the amount of trabecular bone present in the samples is very small since the samples were cut from the mid-diaphysis, some bones contained large porosities present, which were impossible to ignore. These porosities are not visualized in the mesh; however any element which has at least one node in such porosity is put into a different element group and given lower material properties and for convenience, termed a "soft" element. Custom written MATLAB scripts were used to mesh the cortical shells once they have been scanned, and cross-sectional images of the bone were obtained down its entire length (again, with a slice taken at ever 76 microns). The basic algorithm by which the MATLAB script creates the nodes and elements is; (1) use the same threshold value to convert each '.tif' slice into a binary image, (2) find the centroid of the bone in that image, (3) generate ray lines radially outward from the centroid, using pre-defined angular spacing (4) find the first and last point along each ray line which lies on bone material, (5) place a pre-defined number of equally spaced points along each ray line on the bone (6) generate 3D 8-noded elements, using the binary image to determine if nodes are on bone or inside a pore, assigning any element with a node inside a pore lower material properties. Both trabecular and cortical elements are written to text files in Abaqus input file format. All node sets are written to a separate text file, including boundary nodes (the bottom surface) with boundary conditions applied. The model is defined as a linear elastic, orthotropic material, supplying Young's modulus and Poisson's ratio for all principle directions in the cortical. The loading axis of the bone will be given a Young's modulus of 24.76 GPa, while traverse axis modulus will be 17.5 GPa. [3] The "soft" elements will be isotropic and softer, with a Young's Modulus of 0.8 GPa, and poisson's ratio of 0.3.

FE Model Convergence Study

A convergence study was done on a dog femur specimen that was previously used in very similar work. The cortical shell was meshed using the methods described above, with 6 mean spatial resolutions; 0.3, 0.4, 0.5, 0.6, 0.8 and 1 mm. The axial (z-dir) strain measured from the elements at the

Approx. Resolution (R)	Slice # Step	# of Radial Nodes per Ray	# of Rays per 360º
0.3mm	4	9	98
0.4mm	5	6	74
0.5mm	7	5	59
0.6mm	8	5	49
0.8mm	11	3	37
1.0mm	13	3	29

Table 4.1: Convergence study, and corresponding parameters for custom MATLAB meshing program; Slice # Step is the number of slices skipped between the bottom and top of an individual element. The # of radial nodes dictates how many radial layers of elements there will be. And the # of rays per 360º indicates how many elements will mesh the circumferential direction of the cortical shell. These three parameters are calculated from; $\frac{R}{76\mu m}$, $\frac{(outershellradius)-(innershellradius)}{R}$, $\frac{(2*\pi*averageboneradius)}{R}$ respectively.

Strain Gauge 1 location on the cortical bone surface will be used as a convergence measure. This particular region was selected because it reflects the characteristic bending behavior of the cortical diaphysis and it is a key experimental parameter in the PPLL study. Spatial resolutions for the model are estimated through a series of calculations based on the scanner resolution of 76 microns (x,y and z-dir), as shown in Table 4.1. The results seen in Figure 4.1 show a mean resolution of approximately 0.4mm gives good results with minimum computational problem size.

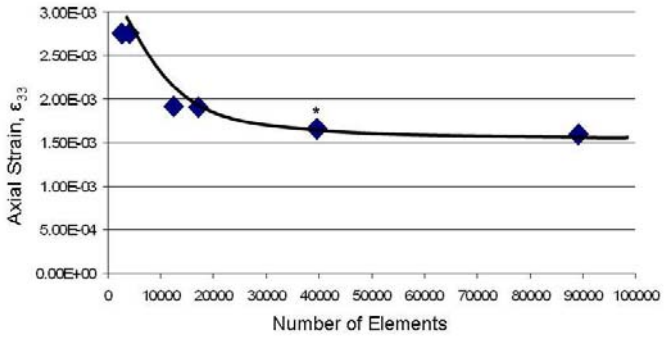

Figure 4.1: Convergence study results. * represents mean spatial resolution of 0.4mm, the chosen resolution for this study. Parameters found here are used to mesh all subsequent bone geometries.

FE Model Loading Protocol and Validation

The cortical shells were experimentally loaded by the MTS machine, and load data was recorded. Since the tests were carried out under load control, the actual force applied was not exactly that desired (due to MTS tuning and feedback controls). The actual load applied by the MTS was taken from the data at each load step. The programmed loads were the 50N reference, and 100 – 800N load steps, while actual loads varied depending on the size of the load step. Each experimental load step will be simulated by creating a load step in ABAQUS. Since the model is linear elastic, and we are assuming small strains, load history is irrelevant, and the load parameters are reset between each step. The total load applied by the MTS is distributed to three nodes on the top surface for loading. This is done to help simulate the possibility of off center loading, or experimentally induced moments. The percent given to each loading node varied from 10-45% of the total applied load. The load node selection and load distribution were varied until the model was considered validated.

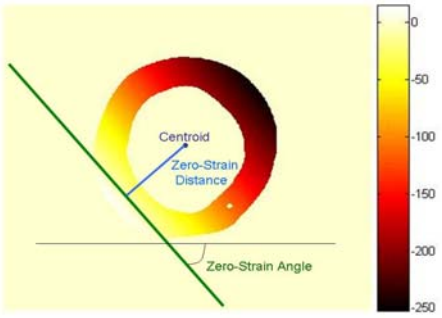

Figure 4.2: 2D axial Strain field and value bar with parameters for FE validation. The Zero-Strain Angle must be within 2 degrees of that calculated from the strain gauges. The Zero-Strain Distance must be within 10% of that measured experimentally.

To validate these models, cortical shells were instrumented with rosette strain gauges during mechanical loading. The strains from these gauges showed good correlation to PPLL frequency changes, further supporting the success of this research. The values of axial strain during each loading phase are used to validate the FE models. Elements on the surface of the

bone in the region of the strain gauge will be used to report axial (e33) strain, extrapolated to the surface nodes. The validation requires the calculation of the 2D strain field in the plane of the gauges, for both experimental and FE data. In these 2D strain fields there exists a "Zero-Strain" axis (Fig. 4.2), where the calculated axial strain is zero (the axis of inflection between compression and tension during bending). First, the angle of this axis compared to the x-axis is calculated, and for proper validation the FE model must be within 2 degrees of the experimental. Second, the distance of this axis to the centroid is calculated, and the FE value must be within 10% of the experimental. Since these 2D strain fields are calculated based on pixel locations in the CT cross-sections, distances are measured in pixels and could be converted to meters based on 76 microns per pixel. Once the zero-axis angle, and distance to centroid are within 2 degrees and 10% respectively, in the final load step (~800N), the model is considered validated.

Data Analysis

The data of interest is the change in length of the ultrasound path through the bone. This data will be correlated to the PPLL frequency to determine whether the strength of the relationship is better than that of the previous chapters. The previous chapters compare PPLL frequency measurements to variables such as force and surface axial strain, and even estimated change in cortical shell thickness based on the 2D axial strain field calculated. The comparison to the actual ultrasound path may provide better relationships to PPLL measurements. The ultrasound path through the bone is a complex topic; therefore three ultrasound paths will be analyzed in each test. The change in the "straight line" path will be calculated as the expansion of the cortical bone shells. In addition to the straight line path, these FE models allow the selection of an arbitrary path, and the extraction of this path length. Two "average" ultrasound paths through the cortical shell, i.e. the paths to the right and left around the shell, along the midline between the endosteal and periosteal surfaces, will be selected in ABAQUS. The comparison of these three paths individually may yield better results when considering that the majority of ultrasound energy may propagate along different paths each time, depending on bone geometry. Each path is manually selected in ABAQUS Viewer (Fig. 4.3). The displacement vectors calculated by ABAQUS for each node along this path during loading will be used to find the overall change in length of this ultrasound path, which will then be used to correlate to the PPLL frequency. Using these

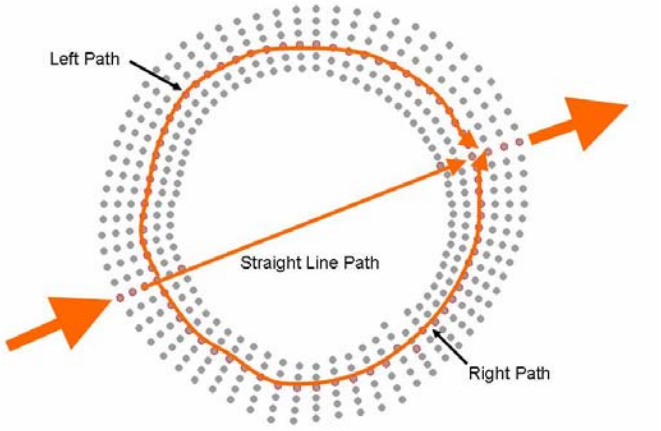

Figure 4.3: Path selection done in ABAQUS. Each node along the desired path is selected and saved in a node set. The order of nodes along the path is recorded and nodal displacement vectors are used to find the length of each path at each load step.

measures of bone dimension will also allow the rough estimation of phase error introduced by the superimposition of the three different ultrasonic paths. Based on absolute node positions, and assumed ultrasound velocities, the phase difference in the signals which travel along the two different paths can be determined. The assumed sound velocity is 3600 m/s in bone and 1450 m/s in the marrow cavity. If the energy from these two paths mixes again before they arrive at the ultrasonic receiving transducer, then the received signal will include artificial phase shift due to this signal interaction. Using the absolute path lengths from ABAQUS, the time of arrival of the energy that travels through each path can be calculated. Then based on the experimental setup of the PPLL, using 2.25 MHz transducers, and 15 cycle bursts, the apparent phase of each signal, and the combined signal can be found.

4.3 Results

First Objective

Seven (7) models were successfully validated according to the parameters set forth for the first objective of this study. Each model represents a single experimental setup, with either marrow or water inside the marrow cavity. The validation parameters for each model are presented in Table 4.2. It is observed that the FE models under linear-elastic assumptions over the entire load range provide similar correlations to PPLL frequency as previously calculated load variables such as axial strain, circumferential strain, and estimated cortical shell thickness change found in chapter 3. (Table 4.3) When comparing previous results to FE model results, the maximum correlation between the three paths can be compared to the

	Δ Zero-Strain Angle	% Zero-Strain Distance
M-13_1	-0.23503	0.3996275
M-13_2	1.974670	-6.966611
M-13_3	0.041071	-0.08331
M-14_3	0.177811	-0.364478
W-11_3	1.618770	7.354615
W-13_2	0.200249	-0.664856
W14_3	-0.70419	0.9485174

Table 4.2: Validation parameters for each model. Zero-Strain angle is presented as difference from experimental (< 2 degrees). Zero-Strain Distance is % off of experimental (<10%).

R^2 Values	FE ΔPs	FE ΔPr	FE ΔPl	EX Axial ε	EX Circ ε	EX Est. ΔCT
M-13_1	0.805	0.810	0.806	0.808	0.858	0.815
M-13_2	0.910	0.910	0.910	0.910	0.900	0.910
M-13_3	0.010	0.010	0.010	0.012	0.022	0.011
M-14_3	0.962	0.962	0.962	0.971	0.906	0.971
W-11_3	0.022	0.022	0.022	0.019	0.003	0.019
W-13_2	0.935	0.942	0.934	0.946	0.910	0.954
W14_3	0.779	0.779	0.779	0.795	0.826	0.794

Table 4.3: R^2 values for the given variable to the PPLL measured frequency. Experimental correlations (EX) are taken from the experiments in chapter 3. Each row is an individual test from Chapter 3, with its corresponding validated FE model. For the FE variables (FE): ΔPs = length change in "straight-line" ultrasound propagation path, ΔPr=length change in the right-hand direction through the cortical shell, ΔPl = length change in the left-hand direction.

estimated change in cortical thickness from the experimental results in chapter 3. We comparing the linear FE models we see an average decrease in correlation to PPLL Frequency of 0.006±0.007, showing no significant difference, and large variation.

Second Objective

Two (2) models were successfully validated for the second objective of this study. These models were validated at each load step in an attempt to model the non-linear properties of the bone. Validation parameters were all within the reduced limits: Δ Zero-Strain Angle < 0.75 degrees, and Zero-Strain Distance within 1%. The main purpose of this objective was to determine if there is a presence of artificial phase artifacts during signal superimposition after propagation through the three main paths.

At a nominal frequency of 2.25 MHz, the wave period is 0.444 μs, and the time it takes for 15 cycles to propagate past a point is 6.666 μs. Thus, if wave energy arrives at the point of signal convergence, there will be a superimposition of these signals, and possible phase artifacts. The times of arrival for the different pathways in the validated model of the experimental test M-13_1, are 11.874 ± 7.87e-5 μs, 8.447 ± 1.75e-4 μs, and 7.339 ± 2.05e-4 μs, for the straight, right and left paths, respectively. For the validated model of experimental test W-14_3, the times of arrival of the different paths are, 11.551 ± 4.06e-4 μs, 9.292 ± 1.73e-4 μs, and 8.074 ± 2.95e-4 μs, for the straight, right and left paths, respectively. The actual time varies with load, since the displacements change, however as seen, the variations are on the order of tenth's of nanoseconds, so only the averages over all steps is presented here. It can be seen that for these two models, there is between a 2 and 5 μs delay between the arrival of the first wave, and the arrival of the last. Therefore, there will in fact be superposition of signals at the point of convergence over at least some of the 15 cycles that the PPLL transmits and receives, as seen in Figure 4.4. Also seen in the superposition of the

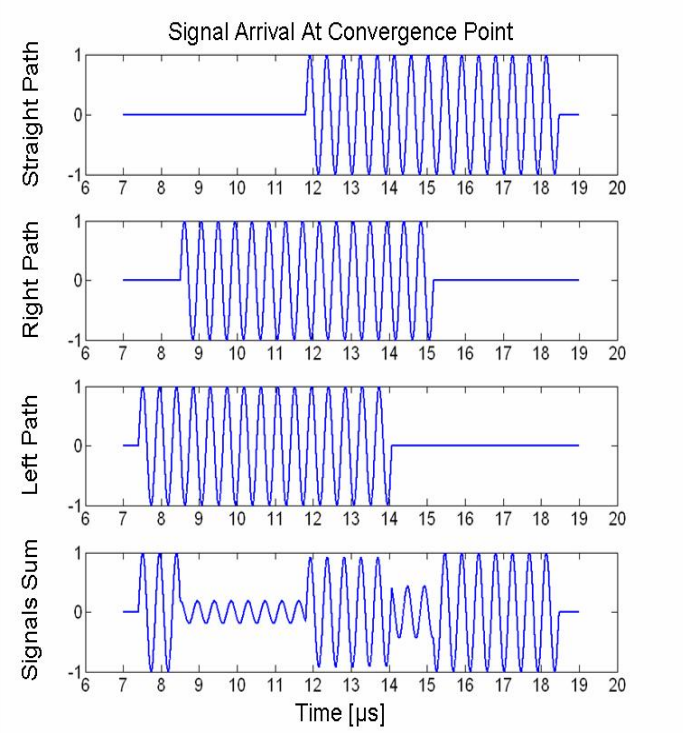

Figure 4.4: Assuming equal and arbitrary sinusoid units, wave energy propagates along separate paths, and arrives at the point of convergence at different times, resulting in possible overlap of several cycles from other paths, resulting in signal superposition. For this example, the left and right paths will interfere with each other over most of their range, while the straight path will add to the two signals in their last few cycles, which can be seen in the plot of the Signal Sum.

signals in Figure 4.3 is the fact that the phase at these different points in the propagating signal will be different due only to this superposition. The apparent phase of the signal when all three pathways combine will vary depending on the load. Even though the time of arrival of the different wave forms vary only slightly, the apparent phase of the combination of the three signals can be greatly effected. The change in this phase artifact is almost linear in these two validated models (R^2 phase vs. MTS applied force ~ 0.93 for M-13_1, and 0.75 for W-14_3) as load is applied. However, the looking at the variation in this phase artifact from the best fit linear line, there is phase discrepancies of up to 2.58 and 2.09 degrees, in the M-13_1 and W-14_3 models respectively. This may seem small, however with PPLL sensitivity in the parts per million, a couple of degrees out of 360, can present large errors.

These two models which approximate the non-linear behavior of the experimental bone can also be used to determine if PPLL frequency more closely relates to the ultrasound propagation paths in these new models. The R^2 values are presented in Table 4.4. Most notably, the R^2 of the PPLL frequency measurements versus the Right-Handed Ultrasound Path Length jumps to 0.993 and 0.879 of models M-13_1 and W-14_3 respectively, while the experimental R^2 to estimated Cortical Shell Expansion was only 0.815 and 0.794, for tests M-13_1 and W-14_3, respectively.

R^2 Values	FE2 ΔPs	FE2 ΔPr	FE2 ΔPl	EX Est. ΔCT
M-13_1	0.307	0.993	0.987	0.815
W14_3	0.796	0.876	0.866	0.794

Table 4.4: R^2 values for the given variable to the PPLL measured frequency.

4.4 Discussion

The use of finite element modeling to obtain geometric parameters along the ultrasound path has shown that there is no one preferred path which the ultrasound would take during ultrasonic measurements through the cortical shell. Rather, the ultrasound is pervasive, and propagates through several different paths, leading to a superposition of signals at the ultrasound receiver. This causes serious problems for through transmission measurements employing the pulsed phase-locked-loop, since this superposition of signals causes artificial phase shifts. While ideally a $\Delta l/l - \Delta f/f$ relationship could be found, the complexities of the ultrasound propagation make this relationship dependent on more than just the change in ultrasound path length.

In the first objective of this work, we can see that using a linear model to approximate our experimental results yields no better relationships to the PPLL measurements. This result is fairly predictable when examining the raw data from the experimental tests. The PPLL frequency measurements are not always linear, and therefore, comparison to linear load variables and a linear FE model will provide similar results. However, these models also do not show any preference for which geometric pathway ultrasound energy may take when propagating through bone. This means that under the linear assumption, ultrasound energy may propagate through all paths evenly. This would result in the maximum amount of signal interference once the signal converged. More interesting, is the fact that this does not appear to be the case when using these linear models to piecewise approximate the non-linear behavior of the bones experimentally.

When validating each load step of the models to more stringent parameters they begin to approximate the nonlinear properties of the bones during experimental loading. In these models it can in fact be seen that the ultrasound may propagate through a preferred path, with much higher correlations seen in one path over another. The PPLL frequency measurements

more are more closely related to the changes in ultrasound path length along one or two preferred paths through the bone, than load variables or axial strain measurements. This is a promising result, since it provides support that the PPLL is in fact measuring changes in ultrasound path length as was over all hypothesized in this work.

Also important is the fact that these stepwise nonlinear approximations allow a more accurate depiction of the phase artifacts due to signal superposition. It can be seen by looking at the geometry of the bone, and making assumptions of wave velocity, that energy may separate and converge again after propagation through three main paths. This convergence has been shown to be very relevant as all energies arrive at the point of convergence within 6.67 μs of each other, resulting in signal superposition, and phase artifacts. This means that the choice of PPLL system lock point in the experimental tests is in fact, very important. Choice of lock point towards the beginning of the 15 propagating cycles means the phase of the temporally shortest path will be most important. If the lock point exists inside the region of the signal where energies superimpose upon each other can result in seeing the effects of this phase artifact. The fact that this phase artifact is close to linear in these two validated models does not make it less of a problem. First, the phase artifact may increase or decrease the actual phase change measured by the PPLL, making system response artificially larger or smaller. This provides problems for any attempts at looking at a $\Delta l/l - \Delta f/f$ relationship. Second, even in these two models where the phase artifact is close to linear, it still varies from its best-fit linear approximation by a maximum or more than 2 degrees. This may seem small, until you take into account that the PPLL system has sensitivity in the parts per million. Thus an artifact that varies somewhat randomly on top of the true signal by about 2 degrees out of 360 can provide enough noise to cause problems to linear relationships.

While a linear approximation is admittedly an inaccurate depiction of bone's nonlinear behavior, it provides a easily attainable estimation of transverse path geometries. Stepwise validating each step allows the approximation of these nonlinear behaviors, but requires 7 times more work. The iterative perturbations of loading distributions to obtain validated load steps can be time consuming. It is also noted that loading only three nodes at the top surface is not experimentally accurate, however since we are not looking at mechanical environments anywhere but in the central region just about the validation level, and stress concentrations at the load surface can be ignored. This finite element modeling work allows us to see that through transmission measurements carry an inherent complexity due to bone geometry and ultrasound energy propagation. The complexities of this methodology makes other measurement mode, such as pulse-echo or longitudinal, much more appealing. The propagation of acoustic energy is not arbitrary, and while continued efforts in this work may show that there is always a singular preferred energy path, the choice of system lock point within a suitable signal region to avoid phase artifacts may still prove difficult. Despite difficulties, the ability to separate out a preferred path to increase correlations to PPLL frequency shows that the PPLL system does in fact closely relate to ultrasound path length changes under ideal conditions and the use of this system to estimate mechanical environment in hard tissue is worthy of further investigation.

Chapter 5: Conclusion and Future Work

To determine whether a system based on the Pulsed Phase-Lock-Loop circuitry could be sensitive enough to detect changes in bone geometry during loading, three main specific aims were proposed. First, the system was tested using geometrically simple phantoms to determine the systems performance under simplistic conditions. Second, the system performance was tested using real bone geometry. And third, FEA models were created to determine if the PPLL more closely tracked actual dimensional changes seen in bone during loading. After concluding the objective the PPLL system has proven able to detect changes in bone during loading.

The system was shown to very closely relate to changes during loading of phantom material. With the most simplistic geometry, a flat faced block, the system was able to track changes during loading with a correlation coefficient of 0.928 ± 0.032. The performance significantly decreased as the geometry became more complicated, most likely due to complex ultrasound propagation patterns.

Utilizing cortical shells cut from sheep femurs, the system was used to take measurements transversely to the load axis during compression testing. With rosette strain gauges, surface strain parameters just below the area of ultrasound penetration were measured at three points around the circumference of the bones. Linear strain fields were calculated in the 2D cross section of the bone where the gauges were attached. The PPLL frequency measurements were found to be moderately related to both axial, and circumferential strain measurements, regardless of marrow cavity contents (Axial Strain, M-group $R^2=0.70\pm0.27$, W-group $R^2=0.62\pm0.29$). This provides good indication that the PPLL is sensitive enough to detect changes in bone during loading; however the variability seen is worth investigation. It is seen that some tests show that PPLL frequency measurements almost completely depends on mechanical loading state, while some tests shows absolutely no relation whatsoever. In investigation into the raw data, it was seen that a number of tests simply had no PPLL system response during loading, despite previously successful tests. There may be several reasons for a lack of system response, which can be broken down into experimental setup error, or ultrasonic signal interference. With experimental setup error, mainly bad connections or water penetrating the transducer wiring, could cause such lack of system response; however is unpredictable and un testable with acquired data, but is also easily mitigated in the future with the proper equipment. Ultrasonic interference also somewhat depends on experimental setup, as the burst widths, signal frequency, and material geometry will all have an effect on the wave propagation. Experimentally looking at a cortical shell with both water, and air inside the marrow cavity, it can be seen that a significant amount of energy can pass through the cortical shell during through transmission. And more importantly, due to the increased velocity in bone versus marrow cavity contents, any signal that passes straight through arrives at roughly the same time as any wave energy that follows the cortical shell. This is cause for concern, as wave energy interference can cause phase shifts and amplitude changes, possibly diminishing the received signal to below noise levels, causing a total lack of system response.

It was then shown using FE models that the PPLL frequency measurements are in fact closely related to the ultrasound path length changes. The spatial changes seen in these FE models were on the order of tens of nanometers to several micrometers. The strong PPLL response at such small levels of ultrasound path length variation shows the great sensitivity

of these PPLL systems, and further justifies their exploration. However, separating out which path is preferred for each individual test can yield slightly stronger relationships, which means the final received signal was most likely largely composed of energy from that path. Wave interference patterns were seen to pose problems based on the current experimental setup. And with phase artifacts that are not necessarily linear, the experimental design becomes ever more important to minimize these effects. Using linear models to stepwise approximate the nonlinear behavior in bone proved to be an effective technique. Since only 8 load steps exist in our experimental design, a maximum of 8 separate load conditions would need to be found via trial and error. True non-linear models can be created for each bone geometry, however for the results important here, simple geometric changes, the stepwise approximations are an easier alternative.

Future works can be done to both better understand the results obtained here, and more importantly, to better understand the functionality of the PPLL technique in monitoring bone strain. Continued validation of more FE models may enhance the results seen in the tracking of the PPLL and distinct ultrasound paths. Trends may arise as to an overall best transmission path for through transmission, however it is noted that due to the other possible propagation paths, great care must be taken in the selection of system lock point. These FE models may also yield information with regards to how much of an effect density changes due to strain may have. In future experiments utilizing the PPLL technique, with its high sensitivity to phase shifts, it is recognized that through transmission is a difficult method to control. Pulse-echo techniques, exploring the expansion of a single cortical shell under loading should provide more consistent results. Through transmission techniques may prove more consistent at sites passing through a large amount of trabecular bone, such as the whole calcaneus. Using a small beam cross-section can allow the majority of energy to propagate relatively straight through the trabecular region, and with proper signal amplification, consistent measurements may be taken using this method. For diagnostic purposes, transmission through trabecular regions holds more functionality, therefore through transmission measurements must be utilized, and suitable sites with minimal signal interference should be found. It is now known that the PPLL technique can provide adequate, perhaps to much, sensitivity to bone dimensional changes during loading and with care in experimental design, future applications could prove this technique a very valuable tool in bone research and disease diagnostics.

References

1. Deng, H.-w. and Y.-z. Liu, *Current Topics in Bone Biology*, ed. H.-w. Deng and Y.-z. Liu. 2005, New Jersey: World Scientific. 528.
2. Martin, R.B., D.B. Burr, and N.A. Sharkey, *Skeletal Tissue Mechanics*. 1998, New York: Springer-Verlag. 392.
3. Liebschner and M. A., *Biomechanical considerations of animal models used in tissue engineering of bone.* Biomaterials, 2004. **25**(9): p. 1697-714.
4. Bensamoun, et al., *Transmission scanning acoustic imaging of human cortical bone and relation with the microstructure.* Clin Biomech (Bristol, Avon), 2004. **19**(6): p. 639-47.
5. Bensamoun, et al., *Spatial distribution of acoustic and elastic properties of human femoral cortical bone.* J Biomech, 2004. **37**(4): p. 503-10.
6. Kremkau, F.W., *Diagnostic Ultrasound: Principles and Instruments*. 6 ed. 2002, Philadelphia: W.B. Saunders Company. 428.
7. Shung, K.K., *Diagnostic Ultrasound: Imaging and Blood Flow Measurements*. 2006, Boca Raton: CRC Press Taylor and Francis. 215.
8. Shmerr, L.W. and Jr., *Fundamentals of Ultrasonic Nondestructive Evaluation: A Modeling Approach*. 1998, New York: Plenum Press. 559.
9. Padilla, et al., *Influence of the precision of spectral backscatter measurements on the estimation of scatterers size in cancellous bone.* Ultrasonics, 2006. **44 Suppl 1**: p. e57-60.
10. Padilla, et al., *Estimation of trabecular thickness using ultrasonic backcatter.* Ultrason Imaging, 2006. **28**(1): p. 3-22.
11. Jenson, et al., *In vitro ultrasonic characterization of human cancellous femoral bone using transmission and backscatter measurements: relationships to bone mineral density.* J Acoust Soc Am, 2006. **119**(1): p. 654-63.
12. Sakata, et al., *Assessing bone status beyond BMD: evaluation of bone geometry and porosity by quantitative ultrasound of human finger phalanges.* J Bone Miner Res, 2004. **19**(6): p. 924-30.
13. Best, R., *Phase-Locked Loops: Design, Simulation and Applications*. 3rd ed. 1997, New York: McGraw Hill.
14. Heyman, J.S., *Pulsed phase locked loop strain monitor*, U.S.P. Office, Editor. 1982, Kazenske; Edward H.: United States.
15. Yost, et al., *Fundamental aspects of pulse phase-locked loop technology-based methods for measurement of ultrasonic velocity.* J Acoust Soc Am, 1992. **91**(3): p. 1456-68.
16. Johnson, R. and W.H.Q. IV., *Apparatus and Method for Monitoring Intracranial Pressure*, U.S.P. Office, Editor. 2001: United States.
17. Vecchio, C.J., I.E. Kibblewhite, and D.E. Kotas, *Technique for Eliminating Ambiguity When Making Pulse-Echo Timing Measurments*, U.S.P. Office, Editor. 1999, Ultrafast, Inc.
18. Froggart, M.E., *Apparatus and Method for Measuring Relative Phase of Signals in a Multiple-Echo System*. 1998, USA represented by NASA: United States.
19. Froggatt and M. E., *Pulsed phase locked loop strain monitor*. 1995, The United States of America as represented by the Administrator of the (Washington, DC): United States.

20. Dechape, M., *Measurement System Using Sonic and Ultrasonic Waves*, U.S.P. Office, Editor. 1988: United States.
21. Wiemann, et al., *Noninvasive measurements of intramuscular pressure using pulsed phase-locked loop ultrasound for detecting compartment syndromes: a preliminary report.* J Orthop Trauma, 2006. **20**(7): p. 458-63.
22. Ueno, et al., *Noninvasive assessment of intracranial pressure waveforms by using pulsed phase lock loop technology. Technical note.* J Neurosurg, 2005. **103**(2): p. 361-7.
23. Steinbach, et al., *Intracranial pressure dynamics assessed by noninvasive ultrasound during 30 days of bed rest.* Aviat Space Environ Med, 2005. **76**(2): p. 85-90.
24. Lynch, et al., *Ultrasonic device for the noninvasive diagnosis of compartment syndrome.* Physiol Meas, 2004. **25**(1): p. N1-9.
25. Ueno, et al., *Cranial diameter pulsations measured by non-invasive ultrasound decrease with tilt.* Aviat Space Environ Med, 2003. **74**(8): p. 882-5.
26. Ueno, et al., *Development of a noninvasive technique for the measurement of intracranial pressure.* Biol Sci Space, 1998. **12**(3): p. 270-1.
27. Ueno, et al., *Noninvasive measurement of pulsatile intracranial pressure using ultrasound.* Acta Neurochir Suppl, 1998. **71**: p. 66-9.
28. Yost, W.T. and J.H. Cantrell, *Constant Frequency Pulsed Phase-Locked-Loop Instrument for Measurment of Ultrasonic Velocity.* Rev. Sci. Instrum., 1991. **62**(10): p. 2451-2456.
29. Prosser, W.H., R.E. Green, and Jr., *Characterization of the Nonlinear Elastic Properties of Graphite/Epoxy Composites Using Ultrasound.* Journal of Reinforced Plastics and Composites, 1990. **9**: p. 162-173.
30. Ueno, T., et al., *Pulsed Phase Lock Loop Technique to Measure Intracranial Pressure Non-Invasively*, in *2003 IEEE Ultrasonics Symposium*. 2003, IEEE.
31. Xia, et al., *Bone surface topology mapping and its role in trabecular bone quality assessment using scanning confocal ultrasound.* Osteoporos Int, 2007. **18**(7): p. 905-13.
32. Camozzi, et al., *Quantitative bone ultrasound at phalanges and calcaneus in osteoporotic postmenopausal women: influence of age and measurement site.* Ultrasound Med Biol, 2007. **33**(7): p. 1039-45.
33. Barkmann, et al., *A method for the estimation of femoral bone mineral density from variables of ultrasound transmission through the human femur.* Bone, 2007. **40**(1): p. 37-44.
34. Stewart, et al., *Long-term fracture prediction by DXA and QUS: a 10-year prospective study.* J Bone Miner Res, 2006. **21**(3): p. 413-8.
35. Pfeil, et al., *Multi-site quantitative ultrasound compared to dual energy X-ray absorptiometry in rheumatoid arthritis: effects of body mass index and inflamed soft tissue on reproducibility.* Rheumatol Int, 2006. **26**(12): p. 1084-90.
36. Malavolta, et al., *Quantitative ultrasound assessment of bone.* Aging Clin Exp Res, 2004. **16 Suppl**(3): p. 23-8.
37. Judex, S., *Application of Strain Gages on Cortical Bone in vivo.*, in *Department of Mechanical Engineering*. 1994, University of Calgary: Calgary.